Cancer Letters 519 (2021) 46–62

Contents lists available at ScienceDirect

Cancer Letters

journal homepage: www.elsevier.com/locate/canlet

Acetylation-induced PCK isoenzyme transition promotes metabolic adaption of liver cancer to systemic therapy

Zongpan Jing [1], Jiajia Gao [1], Jun Li, Fangfei Niu, Lusong Tian, Peng Nan, Yan Sun, Xiufeng Xie, Ying Zhu, Yan Zhao, Fang Liu, Lanping Zhou, Yulin Sun [**], Xiaohang Zhao [*]

State Key Laboratory of Molecular Oncology, National Cancer Center/National Clinical Research Center for Cancer/Cancer Hospital, Chinese Academy of Medical Sciences and Peking Union Medical College, Beijing, 100021, China

ARTICLE INFO

Keywords:
Sorafenib resistance
Protein acetylation
Phosphoenolpyruvate carboxykinase isoform 2
Lysine acetyltransferase 8
Lysosome-related protein degradation
Metabolic adaptation
Acetylproteomics
Phosphoproteomics
Protein posttranslational modifications

ABSTRACT

Sorafenib and lenvatinib are approved first-line targeted therapies for advanced liver cancer, but most patients develop acquired resistance. Herein, we found that sorafenib induced extensive acetylation changes towards a more energetic metabolic phenotype. Metabolic adaptation was mediated via acetylation of the Lys-491 (K491) residue of phosphoenolpyruvate carboxykinase isoform 2 (PCK2) (PCK2–K491) and Lys-473 (K473) residue of PCK1 (PCK1–K473) by the lysine acetyltransferase 8 (KAT8), resulting in isoenzyme transition from cytoplasmic PCK1 to mitochondrial PCK2. KAT8-catalyzed PCK2 acetylation at K491 impeded lysosomal degradation to increase the level of PCK2 in resistant cells. PCK2 inhibition in sorafenib-resistant cells significantly reversed drug resistance *in vitro* and *in vivo*. High levels of PCK2 predicted a shorter progression-free survival time in patients who received sorafenib treatment. Therefore, acetylation-induced isoenzyme transition from PCK1 to PCK2 contributes to resistance to systemic therapeutic drugs in liver cancer. PCK2 may be an emerging target for delaying tumor recurrence.

1. Introduction

Liver cancer is the sixth most frequently diagnosed cancer worldwide [1]. Due to the high malignancy and asymptomatic characteristics of liver cancer, >60% of patients present with intermediate stage or advanced stage cancer at diagnosis and have a poor prognosis [2]. Thus, liver cancer is the fourth leading cause of cancer death, accounting for 8.2% of the total cancer deaths [1]. Because the risk factors are continually prevalence, the overall burden of liver cancer is increasing over time [2].

Currently, for patients who have advanced disease, systemic therapies are recommended. Sorafenib was the first approved first-line systemic therapy with the ability to improve survival in liver cancer [3]. Sorafenib is a multiple tyrosine kinase inhibitor that targets up to 40 kinases, including vascular endothelial growth factor receptors (VEGFRs), platelet-derived growth factor receptor-β (PDGFRβ) and intracellular Raf family kinases (predominantly c-Raf rather than B-Raf) [3]. In the SHARP trial, compared with placebo, sorafenib improved median overall survival by 2–3 months [4]. Notably, less than 30% of patients could benefit from sorafenib treatment [5].

Except for primary resistance, most patients develop acquired resistance within 6 months [6]. Over the past decade, abnormal activation of several signaling pathways and processes, including hypoxia, autophagy, PI3K/AKT pathways, epithelial-mesenchymal transition (EMT) and the immune microenvironment, in malignant cells and the tumor microenvironment was found to participate in the initiation and development of sorafenib resistance in liver cancer [6,7]. Unfortunately, due to the complex pharmacological effect of sorafenib, there is currently no available biomarker to predict the therapeutic response to sorafenib in the clinic.

In 2018, the second first-line systemic therapy drug, lenvatinib, was approved for the treatment of liver cancer based on the phase III REFLECT trial, which showed that lenvatinib is not inferior to sorafenib [8]. Lenvatinib is also a multiple tyrosine kinase inhibitor that targets VEGFRs, fibroblast growth factor receptors (FGFRs), PDGFRα, RET and KIT [2]. Importantly, the objective response rate of lenvatinib was

* Corresponding author. State Key Laboratory of Molecular Oncology, Cancer Hospital, Chinese Academy of Medical Sciences, Beijing, China.
** Corresponding author. State Key Laboratory of Molecular Oncology, Cancer Hospital, Chinese Academy of Medical Sciences, Beijing, China.
E-mail addresses: ylsun@cicams.ac.cn (Y. Sun), zhaoxh@cicams.ac.cn (X. Zhao).
[1] These authors contributed equally.

https://doi.org/10.1016/j.canlet.2021.06.016
Received 17 March 2021; Received in revised form 2 June 2021; Accepted 17 June 2021
Available online 21 June 2021

24.1% according to modified RECIST (mRECIST) criteria when evaluated by investigators but reached 40.6% upon independent imaging review [5]. Thus, it is significantly superior to sorafenib. However, thus far, studies on the underlying mechanisms of resistance to lenvatinib are lacking.

Metabolic reprogramming, as one of the hallmarks of cancer, is a fundamental process in tumor tissues [9]. Cancer cells preferentially use glycolysis for energy production, a phenomenon termed the "Warburg effect". In recent years, a few studies focused on sorafenib-induced alterations in central carbon metabolism (glycolysis, gluconeogenesis, the pentose phosphate pathway, and the citric acid (TCA) cycle) in liver cancer. It was found that sorafenib hinders oxidative phosphorylation and stimulates glycolysis in glucose-grown cells [10,11]. The cytotoxicity of sorafenib is dramatically increased by glucose withdrawal or a glycolytic inhibitor [12–14]. A study performed in 2013 reported that enhanced glycolysis or suppression of oxidative phosphorylation is associated with resistance to sorafenib in Huh7 cells [15]. However, a recent study showed a contradictory result: sorafenib-resistant Huh7 cells underwent a switch from glycolysis to oxidative phosphorylation [16]. Currently, it remains unknown how sorafenib, as a multikinase inhibitor, remodels cellular metabolic status. Therefore, systematically elucidating the mechanism of metabolic reprogramming in the context of sorafenib resistance would help to identify new predictive biomarkers for the efficacy of sorafenib treatment and develop novel drugs and even dietary interventions to be used in combination with sorafenib.

Notably, glucose concentrations in tumor tissues are frequently 3- to 10-fold lower than those in adjacent normal tissues and can even be close to zero [17]. Cancer cells adapt their metabolism to mainly rely on mitochondrial oxidative phosphorylation for optimal proliferation [17]. In addition to generating energy, alternative metabolic pathways, such as "abbreviated" gluconeogenesis, can rescue the lack of metabolic intermediates that results from a reduction in glycolytic flux [18–20]. Under low-glucose conditions, gluconeogenesis utilizes nonglucose substrates termed alternative carbon sources, such as lactate, glutamine and amino acids, to generate many of the intermediates of glycolysis. The key rate-limiting gluconeogenic enzyme phosphoenolpyruvate carboxykinase (PEPCK) has been found to play a pivotal role in "abbreviated" gluconeogenesis pathways [18].

In mammals, there are two PEPCK isoenzymes with similar kinetics, namely, a cytosolic isoform PCK1 (also known as PEPCK-C) and a mitochondrial isoform PCK2 (also known as PEPCK-M). PEPCK irreversibly converts oxaloacetate into phosphoenolpyruvate (PEP) in the presence of GTP. PCK1 expression is specific to the liver, kidney, gastrointestinal tract and adipose tissue, whereas PCK2 is ubiquitously expressed in various tissues [21]. In the human liver, the PCK1:PCK2 ratio is approximately 1:1. Intracellular PEP is involved in at least four anabolic pathways, including gluconeogenesis, glyceroneogenesis, serine synthesis and the pentose phosphate pathway [18].

Here, we elucidated the molecular mechanism underlying metabolic reprogramming in sorafenib-resistant HepG2 (HepG2-R) liver cancer cells using integrated multilevel proteomics analyses. Extensive alterations in protein acetylation that are enriched in central carbon metabolism pathways were observed in sorafenib-resistant cells. Further mechanistic studies indicated that the isoenzyme transition from PCK1 to PCK2, which was reciprocally regulated by lysine acetylation at a novel site, endowed cells with a survival advantage and contributed to an acquired resistance phenotype.

2. Materials and methods

2.1. Cell lines and cell culture

HEK 293 and human liver cancer cell lines HepG2 were obtained from the American Type Culture Collection (ATCC; Rockville, MD, USA); Huh-7, Bel-7402, Bel-7404 and SMMC-7721 and L02 cells were purchased from the Institute of Biochemistry and Cell Biology of Chinese Academy of Sciences (Shanghai, China). All cells were authenticated by DNA fingerprinting analysis using STR profiling. And cells were maintained under recommended conditions.

Sorafenib, regorafenib, lenvatinib, rapamycin, 3-mercaptopicolinic acid (3-MPA), histone deacetyltransferase inhibitor (HDACi) and cycloheximide (CHX) were administered as described in the figure legends. A full list of antibodies and reagents can be found in the Key Resources Table (Supplementary Table S1).

To establish HepG2 sorafenib-resistant (HepG2-R) cells, sorafenib (Biovision) was gradually added to the culture medium at a concentration ranging from 1 μM to 15 μM. After 3 months of screening, HepG2-R cells were obtained and maintained in culture medium with 10 μM sorafenib. To generate HepG2 lenvatinib-resistant cells, lenvatinib (Selleck Chemicals) was gradually added to the culture medium at a concentration ranging from 10 μM to 50 μM. After 1 month of screening, lenvatinib-resistant cells were obtained and maintained in culture medium with 50 μM lenvatinib.

2.2. Plasmid construction and transfection

cDNA of the human PCK2, PCK1, KAT8 and KAT5 genes was separately cloned into the indicated vectors. Point mutations in PCK2 (K108R) and PCK2 (K491R) were generated by site-directed mutagenesis. In addition, two lentivirus short hairpin (sh) RNAs targeting PCK2 (shPCK2-1: 5′-GGTGATTGTAACTCCTTCTCA-3'; shPCK2-2: 5′-GCTACAATCCAGAGTAACACT-3′) or a shRNA with a scrambled sequence (5′-ACAGAAGCGATTGTTGATC-3′) was individually inserted into a shRNA vector pLent-U6-GFP-Puro (Vigenebio, Shandong, China). The sequences of siRNAs targeting PCK2 were as follows: siPCK2-1 (5′-GGUGAUUGUAACUCCUUCUCA-3′) or siPCK2-2 (5′-GCUACAAUCCAGAGUAACACU-3′) and siRNAs with the scrambled sequence Scr (5′-UUCUCCGAACGUGUCACGU-3′). For transient transfection, 5×10^5 cells/mL were first plated in a 6-well plate and incubated for 24 h at 37 °C. Then, the cells were transfected with the relevant plasmids using Lipofectamine 3000 (Invitrogen) when cell confluence reached 80%.

2.3. Multi-level proteomics experiments

First, HepG2-WT and HepG2-R cells were pretreated with 10 μM sorafenib for 24 h. Then, the cell samples were separately sonicated on ice in lysis buffer with 8 M urea, digested with trypsin, desalinated and labeled with TMTsixplex™ (Thermo Scientific, Waltham, MA, USA). The labeled peptides were mixed and divided into 3 samples each to quantify total protein, acetylated protein and phosphorylated protein levels.

HPLC separation was performed using a Thermo Betasil C18 column (5 μm particles, 10 mm ID, 250 mm length); acetylated peptides were immunoprecipitated by with a pan-acetylation antibody (Cat#: PTM104, PTM-Bio, Hangzhou, China), and phosphoryl-peptides were enriched by immobilized metal affinity chromatography (IMAC) and immunoprecipitated by an anti-phospho-tyrosine antibody (Cat # PTM1001, PTM-Bio, Hangzhou, China). The EASY-nLC 1000 UPLC system (Thermo Fisher Scientific), Q Exactive™ Plus (Thermo Fisher Scientific) and MaxQuant search engine (v. 1.5.2.8) were used to identify and quantify peptides. Trypsin/P was specified as a cleavage enzyme allowing up to 4 missing cleavages. The mass tolerance for precursor ions was set as 20 ppm in the first search and 5 ppm in the main search, and the mass tolerance for fragment ions was set as 0.02 Da. Carbamidomethylation of Cys residues was specified as a fixed modification, and acetylation, phosphorylation and oxidation of Met residues were specified as variable modifications. The FDR was adjusted to <1%, and the minimum score for modified peptides was set as > 40.

For analysis of proteomics data, proteins or peptides with fold changes ≥1.2 between HepG2-WT and HepG2-R cells and $p < 0.05$ by Student's *t*-test were considered significantly altered. Gene Ontology (GO) annotation was derived from the UniProt-GOA database (www.http://www.ebi.ac.uk/GOA/). The Encyclopedia of Genes and Genomes

(KEGG) (https://www.kegg.jp/) database was used to identify enriched pathways.

2.4. Western blot analysis

Cells were lysed in RIPA lysis buffer supplemented with protease inhibitor cocktail (Roche, Basel, Switzerland) and phosphatase inhibitor cocktail (Bimake, Houston, TX, USA) without HDACi. Then, the proteins were separated by SDS-PAGE and transferred onto a PVDF membrane (Millipore, Billerica, MA, USA). The membranes were blocked with 10% skim milk at room temperature for 3 h, incubated with primary antibodies overnight at 4 °C, washed with TBST three times and incubated with HRP-conjugated secondary antibodies at room temperature for 1 h. Protein bands were visualized using Super Signal West Femto Maximum Sensitivity Substrate (Thermo Fisher Scientific), and exposure images were taken with the ImageQuant LAS4000 mini system (GE, Boston, MA, USA).

2.5. Immunoprecipitation assay

Total proteins were extracted with NP-40 lysis buffer (150 mM NaCl, 50 mM Tris-HCl (pH 7.5) and 1% NP-40) supplemented with protease inhibitor and phosphatase inhibitor cocktails without HDACi. Primary antibody or control IgG was incubated with Dynabeads Protein G (Thermo Fisher Scientific) at room temperature for 1 h. Then, the Dynabeads Protein G-Ig complex was washed twice in 1 ml of 0.2 M triethanolamine (pH 8.2) and incubated in 1 ml of fresh 0.2 M triethanolamine (pH 8.2) with 20 mM dimethyl pimelimidate (DMP)-2HCl for 30 min at room temperature with end-over-end rotation to crosslink the antibody to the beads. After crosslinking, 500 μL of protein lysate was mixed with the antibody-Protein G bead complex and incubated overnight at 4 °C with end-over-end rotation. The beads were then washed 5 times with 1 mL of 0.1% NP40 lysis buffer supplemented with protease inhibitors. Finally, the immunoprecipitated proteins were dissolved in 1 × SDS loading buffer and subjected to Western blotting.

2.6. RNA extraction and quantitative PCR

After total RNA extraction with TRIzol reagent (Invitrogen), the HiFiScript cDNA Synthesis Kit (CWbiotech, Jiangsu, China) was used to perform reverse transcription. Then, SYBR Green Real-Time PCR Master Mix (Takara, Dalian, China) was used to carry out quantitative PCR on an ABI Quant Studio 5 device (Applied Biosystems). Relative mRNA levels were determined by the cycle threshold (Ct) and normalized to *ACTB* levels using the $2^{-\Delta\Delta Ct}$ method. The primer sequences are shown in Supplementary Table S2.

2.7. Xenograft model

Four-week-old female NCG mice were obtained from GenPharmatech (Nanjing, Jiangsu, China) and housed in a virus/antigen-free facility. A total of 5×10^6 HepG2-R-shPCK2-1, HepG2-R-shPCK2-2 or HepG2-R-shCtrl cells were suspended in 100 μL of 1 × PBS and injected into the flanks of NCG mice from three groups (n = 12/group). The tumor volume (TV) was calculated as follows: TV = 0.5 × length × width^2. When the average TV reached 50 mm^3, the 3 groups mice were divided into 6 groups (n = 6/group); 3 groups of NCG mice were intragastrically administered 30 mg/kg sorafenib dissolved in 100 μL corn oil every day for 17 days, and the other 3 groups were administered DMSO dissolved in 100 μL corn oil every day for 17 days. Body weight and TV were measured every 3 days. Thirty-eight days after cell injection, the mice were euthanized, and the tumors were dissected. The tumors were weighed and fixed in 4% formaldehyde and then embedded and sectioned. All experimental procedures were approved by the Institutional Animal Care and Use Committee (IACUC) of Cancer Hospital of Chinese Academy of Medical Science.

2.8. Flow cytometry

A total of 2×10^6 cells/well were seeded in 6-well plates until they reached 60% confluence. The cells were treated with the indicated drugs for 48 h and digested with 0.05% EDTA-free trypsin (Cell Technologies). After washing with 1 × PBS, the cells were incubated with Annexin V-FITC and propidium iodide (PI) (4A Biotech, Beijing, China). The ratio of apoptotic cells was determined with a BD LSRII flow cytometer (BD Biosciences, Franklin Lakes, NJ, USA).

2.9. Short-term colony formation

A total of 2×10^6 cells/well was seeded in 6-well plates. Twenty-four hours later, culture medium containing the indicated drugs was added to each well. After 48 h of treatment, the cells were fixed with 4% paraformaldehyde (PFA) and stained with 1% crystal violet, and colonies were counted. All experiments were performed in triplicate, and the results are presented as the mean ± SEM.

2.10. Cell viability

For cell viability assays, 2×10^4 cells/well were seeded in white clear-bottom 96-well plates (Corning) and allowed to reach 40% confluence prior to treatment with drugs at different concentrations of the drugs as indicated in the figure legends. Culture medium containing the indicated drugs was added to each well, and each treatment group contained 8 replicates. After incubation for 48 h, 10 mL of CCK-8 reagent was added to each well, and the cells incubated for 2 h at 37 °C. Cell viability was measured according to the optical density (OD) at 450 nm, and the IC_{50} value was defined as the drug concentration that inhibited 50% of cell growth compared with the untreated control. This value was calculated using Prism 5.0 software (GraphPad Software, San Diego, CA, USA) according to the following formula: cell proliferation rate (%) = (OD450 with drug/OD450 with control) × 100%. Finally, the absorbance at 450 nm was measured using a microplate reader to evaluate cell viability. All experiments were performed in triplicate, and the results are presented as the mean ± standard error of the mean (SEM).

2.11. Immunofluorescence staining

Cells growing on coverslips in 6-well plates (Corning) were fixed with 4% paraformaldehyde for 20 min and permeabilized for 20 min with 0.2% Triton X-100 after being washed three times with PBS. After the cells were blocked with 2% BSA for 2 h at room temperature, they were incubated overnight with the appropriate primary antibodies at 4 °C. Then, the cells were incubated with the corresponding Alexa Fluor 488- or Alexa Fluor 594-conjugated secondary antibodies (Thermo Fisher Scientific) at room temperature for 1 h. Finally, the cell nuclei were stained with 6-diamidino-2-phenylindole (DAPI) solution (Sigma-Aldrich). Fluorescence images were captured with a laser scanning confocal microscope (PerkinElmer).

2.12. Mitochondrial respiration ability

Mitochondrial respiration was measured using the Agilent Seahorse XF Cell Mito Stress Test Kit (Agilent) following the manufacturer's protocol. Briefly, a total of 2×10^4 cells were seeded in each well of a Seahorse XF96 Cell Culture Microplate and incubated for 24 h at 37 °C. Subsequently, the baseline oxygen consumption rate (OCR) and OCR under pressure were measured with a Seahorse XFe96 Analyzer during sequential addition of the indicated drugs, i.e., 2 μM oligomycin, 2 μM FCCP and 0.5 μM rotenone/antimycin A.

2.13. Lysosome isolation

Lysosomes were isolated from 2×10^7 cells by using a lysosome

isolation kit (Invent Biotechnologies, Plymouth, MN, USA) according to the manufacturer's instructions. Briefly, after cell homogenization, cell debris was removed by centrifugation at 2000×*g*. The supernatant obtained in the last step was centrifuged at 12,000×*g* to isolate mitochondria (low purity), and the supernatant obtained in the last step was centrifuged at 16,000×*g* to isolate lysosomes.

2.14. Immunohistochemical staining

HCC tissue microarrays (Superbiotek, Shanghai, China) or slides of tumors from xenografts were analyzed using immunohistochemistry (IHC) to assess the expression level of PCK2 *in vivo*. Briefly, formalin-fixed and paraffin-embedded tumor tissues were deparaffinized, rehydrated at room temperature, and immersed in methanol containing 0.3% hydrogen peroxide for 10 min to block endogenous peroxidase activity. Heat-induced antigen retrieval was performed in antigen retrieval solution at pH 6.0 in a water bath for 30 min. After washing, the sections were incubated with primary antibody at 4 °C overnight. After washing with 1 × PBS, the slides were reacted with the Prolink-2 Plus HRP Rabbit Polymer Detection Kit (Golden Bridge, Bothell, WA, USA) according to the manufacturer's instructions. Images were taken using Aperio ScanScope CS software (Aperio Technologies, Vista, CA, USA). The microarrays were evaluated and scored based on the intensity and extent of staining. Briefly, PCK2 staining intensity scores (0, negative; 1, weak; 2, moderate; and 3, strong) and staining area scores (0, 0–5%; 1, 6–25%; 2, 26–50%; 3, 50–75%; and 4, >75%) were multiplied to generate the total score; a total score = 12 was considered high expression, and a total score < 12 was considered low expression.

2.15. Enzyme activity

Phosphoenolpyruvate carboxykinase (PEPCK) enzyme activity was measured using the Phosphoenolpyruvate Carboxykinase Activity Assay Kit (Biovision, Milpitas, CA, USA) according to the manufacturer's instructions. In this assay, PEPCK catalyzed the conversion of phosphoenolpyruvate (PEP) to oxaloacetate (OAA). After a series of transitions under a set of enzymes, the OD at 570 nm was measured, and the OAA concentration was calculated.

2.16. GST pulldown assay

PCK2 (expressed by and purified from *E. coli.*) fused with GST or GST-KAT8 was incubated in NP-40 buffer overnight at 4 °C. The complex was then added to glutathione magnetic beads. After washing 5 times, binding proteins were eluted with 1 × SDS loading buffer at 95 °C, and then Western blot analysis was performed.

2.17. Quantification and statistical analysis

All experiments were repeated independently at least 3 times, and quantitative data are shown as the means ± standard deviations (SDs)/SEMs. GraphPad Prism 8 software (GraphPad Software, San Diego, CA, USA) was used for statistical analysis, and the tests used for analysis are indicated in the figure legends. ns, not significant; $^{*}P < 0.05$, $^{**}P < 0.01$, $^{***}P < 0.001$ and $^{****}P < 0.0001$ were considered statistically significant.

2.18. Data availability

The MS proteomics data have been deposited to the ProteomeXchange Consortium (http://proteomecentral.proteomexchange.org) via the iProX partner repository with the dataset identifier PXD022937. All datasets generated are available from the corresponding author upon request.

3. Results

3.1. Sorafenib-resistant liver cancer cells exhibited metabolic features of increased glycolysis and oxidative phosphorylation

To mimic the acquired resistance to sorafenib observed in clinical specimens, a HepG2-R subline was generated by successively exposing wild-type (HepG2-WT) cells to increasing doses of sorafenib. During the induction of resistance, HepG2-R cells exhibited morphological and molecular changes associated with EMT, which was consistent with previous studies (Fig. 1A) [16,22]. The resistance phenotype was characterized by measuring sensitivity to sorafenib and subjecting resistant and control cells to cell apoptosis and clonogenic assays. HepG2-R cells were 3.2 times more resistant to sorafenib than HepG2-WT cells; the IC_{50} value of sorafenib was 26.20 ± 1.10 μM in HepG2-R cells and 8.23 ± 1.09 μM in HepG2-WT cells (Fig. 1B). Sorafenib dramatically induced apoptosis and inhibited colony formation in HepG2-WT cells in a dose-dependent manner, whereas the number of apoptotic cells was significantly diminished in HepG2-R cells, resulting in improved cell survival (Fig. 1C and D). Thus, we successfully established a cell model of acquired resistance to sorafenib.

Furthermore, we observed striking metabolic alterations in HepG2-WT cells exposed to sorafenib. Measurement of mitochondrial respiration using a Seahorse XF analyzer showed that basal oxidative phosphorylation, maximal respiration, and spare respiratory capacity were dramatically reduced by sorafenib (Fig. 1E). When the cell energy phenotype was assessed, we found that compared with HepG2-WT, HepG2-R cells were more energetic in the resting state, as they consumed more oxygen and exhibited greater glycolytic function. In the presence of sorafenib, HepG2-WT cells were completely quiescent. Moreover, HepG2-R cells maintained some respiration activity, although they exhibited a drastic decrease in oxygen consumption and the glycolytic response (Fig. 1F). Collectively, these findings suggest that sorafenib-resistant cells acquired a more energetic phenotype with enhanced mitochondrial respiration and glycolysis activity to adapt to the inhibition of oxidative phosphorylation by sorafenib.

3.2. Characterization of the metabolic alterations in sorafenib-resistant cells by multilevel proteomics analyses

Given that sorafenib is a multiple tyrosine kinase inhibitor, we subjected HepG2-WT and HepG2-R cells to integrated proteomics, phosphoproteomics and acetylproteomics analyses to elucidate the mechanism of metabolic reprogramming in sorafenib-resistant cells (Fig. 1G). Quantitative proteomics analysis identified a total of 4984 proteins, with 4365 proteins having a 1% false discovery rate at both the peptide and protein levels. Phosphoproteomics analysis identified a total of 7459 phosphosites corresponding to 2508 phosphoproteins, 70.4% (5250) and 81.8% (2051) of which, respectively, could be quantified. Using the criteria of a fold change greater than 1.3 and a *P* value less than 0.05, 350 and 136 phosphosites mapping to 275 and 124 phosphoproteins was identified as being increased and decreased, respectively (Supplementary Table S3). Acetylproteomics analysis revealed a total of 895 acetylated sites, corresponding to 543 acetylated proteins, 91.1% (815) and 92.6% (503) of which, respectively, could be quantified. Using the criteria of a fold change greater than 1.3 and a *P* value less than 0.05, acetylation of 234 and 30 sites from 179 to 18 acetylated proteins was identified as being increased and decreased, respectively (Supplementary Table S3).

To assess the biological relevance of the differentially expressed phosphoproteins and acetylated proteins, we constructed integrative functional networks according to KEGG pathway enrichment analysis. For the differentially expressed phosphoproteins (Fig. 2A), the enriched pathways were mainly in the module of pathways known to be regulated by sorafenib. The HIF-1 signaling pathway has also been reported to be associated with sorafenib resistance. These results agree well with those

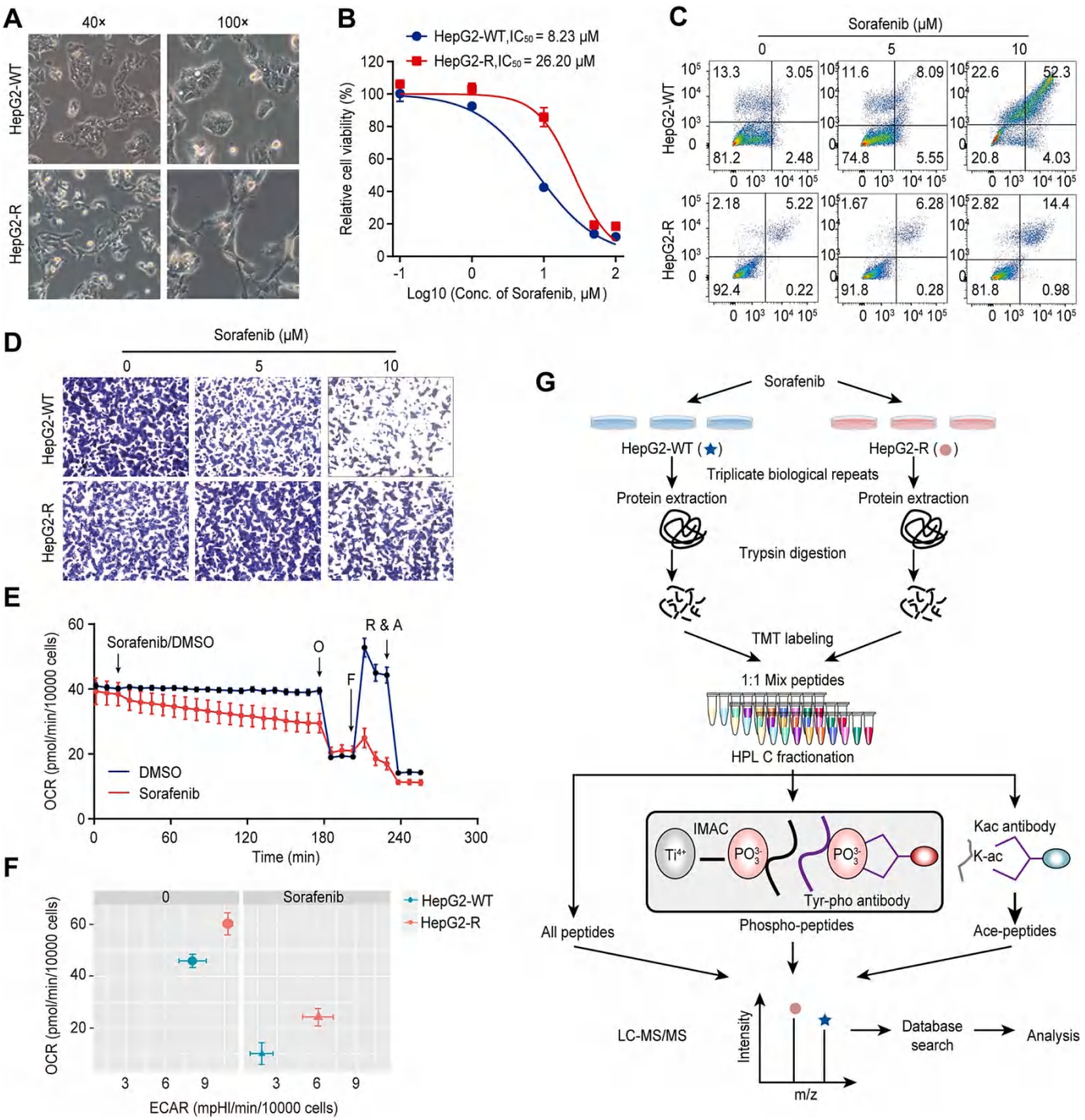

Fig. 1. HepG2-R cells exhibited significant metabolic alterations. (A) HepG2-R cells presented different morphological characteristics than HepG2-WT cells, displaying a spindle shape and pseudopodia formation that was consistent with an EMT phenotype. (B) Concentration-response plot of HepG2-WT and HepG2-R cells to sorafenib, as determined by the CCK-8 assay. (C) HepG2-R and HepG2-WT cells were incubated with the indicated concentrations of sorafenib (0, 5 μM and 10 μM) for 48 h, and cell death was quantified by flow cytometry analysis of Annexin V/PI fluorescence. (D) Images showing crystal violet-stained HepG2-WT and HepG2-R cells. The cells were treated with different concentrations of sorafenib (0, 5 μM and 10 μM) for 48 h, fixed and stained with crystal violet. (E) Seahorse XF mitochondrial stress analysis showed that treatment with 5 μM sorafenib for 4 h acutely inhibited ATP-linked oxygen consumption in HepG2-WT. DMSO was used as a negative control (NC). (F) Seahorse XF cell energy phenotype analysis of HepG2-WT and HepG2-R cells in the absence or presence of 5 μM sorafenib for 4 h. The Y-axis represents the oxygen consumption rate (OCR, mitochondrial respiration), and the X-axis represents the extracellular acidification rate (ECAR, glycolysis). (G) Workflow of the proteomics, phosphoproteomics and acetylproteomics analysis of HepG2-WT and HepG2-R cells. Both HepG2-WT and HepG2-R cells were treated with 5 μM sorafenib for 24 h before cell lysis. Different batches of protein extracted from both types of cells served as biological triplicates. After trypsin digestion in solution, the peptides were labeled with TMT 6-plex reagent. The peptides were then mixed and separated into 60 fractions through off-line high pH RP chromatography. For proteomics analysis, 60 fractions were combined into 18 fractions. For phosphoproteomics and acetylproteomics analysis, 60 fractions were combined into six fractions and then dried in a speed vacuum. After peptide reconstitution in IP buffer, phosphopeptides and acetylpeptides were enriched by immobilized metal affinity chromatography (IMAC) and immunoprecipitation with anti-phospho-tyrosine and anti-pan-acetylation antibodies. The eluted peptides were injected into the mass spectrometer for protein identification and quantification.

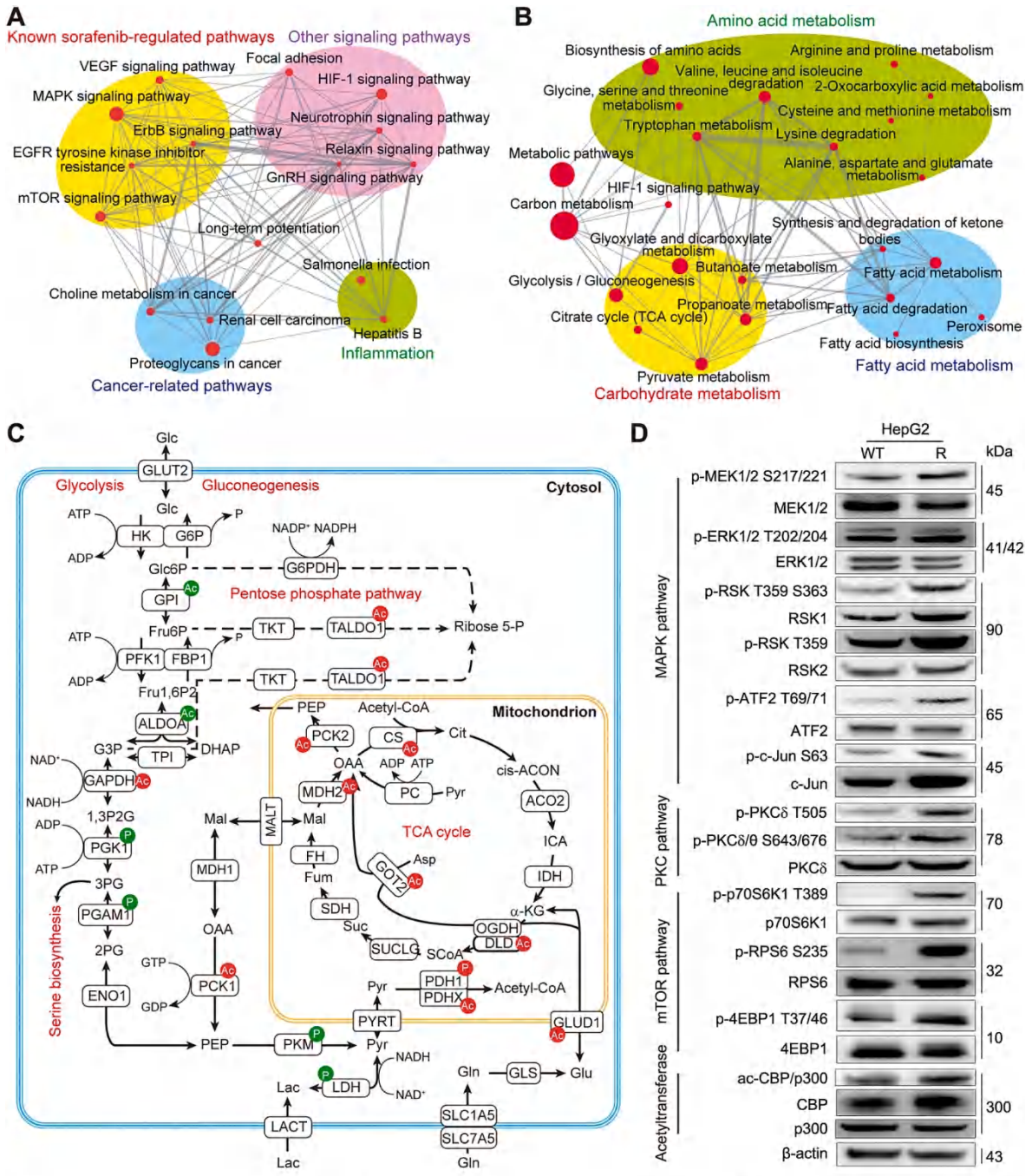

(caption on next page)

Fig. 2. Enrichment analysis and validation of differentially expressed phosphoproteins and acetylated proteins in sorafenib-sensitive HepG2 cells and -resistant HepG2-R cells. (A–B) Network analysis of KEGG pathways for which differentially expressed phosphoproteins (A) and acetylated proteins (B) were enriched. The pathways are grouped by the known functions. The size of each node represents the -log10 (*P* value) of that pathway. Interactions between pairs of pathways are indicated by edges. Thicker edges represent more overlapped proteins. (C) Sorafenib resistance-related differentially expressed proteins were enriched in carbohydrate metabolism pathways. The carbohydrate metabolism pathways in the schematic diagram include glycolysis, gluconeogenesis, TCA cycle, lactic acid and glutamine gluconeogenesis, and the pentose phosphate pathway. The intermediates of gluconeogenesis can enter the pentose phosphate pathway for the biosynthesis of ribose 5-phosphate and nucleotides. The phosphorylation and acetylation modifications of metabolic enzymes that were increased in sorafenib-resistant cells are marked in red, while the PTMs that were decreased are marked in green. The increases and decreases were normalized to the corresponding protein level. (D) Western blot analysis of several important differentially expressed phosphorylated and acetylated proteins in HepG2-WT (WT) and HepG2-R (R) cells. β-Actin was used as an internal control. (E) Rapamycin and sorafenib had a synergistic effect. HepG2-R cells (2×10^4) were seeded in each well in 96-well plates and cultured for 24 h. Then, the viability of HepG2-WT cells in the presence of the indicated concentrations of sorafenib alone or sorafenib combined with rapamycin (1:1) was assessed for 48 h. (F) Viability of HepG2-R cells in the presence or absence of 2 mM glutamine in the culture media for 48 h. (G) Lactate consumption rates of HepG2-WT and HepG2-R cells in medium comprising 0 mM glucose and 5 mM lactate for the indicated times. For (E–G): **, $P < 0.01$; ***, $P < 0.001$; and ****, $P < 0.0001$.

of the previous studies. Intriguingly, we found abnormal alterations in the acetylation of a wide range of metabolic enzymes in HepG2-R cells (Fig. 2B). These alterations are involved in carbon metabolism, carbohydrate metabolism, amino acid metabolism and fatty acid metabolism.

Given the metabolic alterations in HepG2-R cells, we focused on the glycolysis/gluconeogenesis pathway and TCA cycle. As shown in Fig. 2C, the acetylation levels of several enzymes in mitochondria were significantly increased. To verify the reliability of the multilevel proteomics analyses, the expression of several differentially expressed proteins was analyzed by Western blotting (Fig. 2D). It was confirmed that the expression of the phosphorylated forms of MEK1/2, RSK1/2, ATF2, c-Jun, PKCδ, p70S6K1, RPS6 and 4EBP1 as well as acetylated CBP/p300 were upregulated in HepG2-R cells, which was in line with the proteomics results.

In addition, because the mTOR pathway was activated in sorafenib-resistant cells, we validated the effect of the combination of sorafenib and the mTOR inhibitor rapamycin. As reported previously [23], coadministration significantly increased the death of HepG2-WT cells (Fig. 2E).

3.3. Alternative carbon sources were utilized by sorafenib-resistant cells

TCA cycle is the hub for energy metabolism and biosynthesis, and intermediates contribute to anabolism via anaplerosis, especially for gluconeogenesis and the pentose phosphate pathway. Therefore, we first evaluated the utilization of alternative carbon sources. In HepG2-R cells, glutamine deprivation decreased cell viability in the presence of sorafenib; that is, sorafenib-resistant cells exhibited glutamine addiction (Fig. 2F). Next, in the absence of glucose, sorafenib-resistant cells consumed more lactate as fuel than HepG2-WT cells (Fig. 2G). Thus, active gluconeogenesis from glutamine and lactate enhanced tolerance to sorafenib.

3.4. Isoenzyme transition from PCK1 to PCK2 contributed to sorafenib resistance

Because of the critical roles of alternative carbon source utilization and gluconeogenesis, we concentrated on the rate-limiting enzyme of the gluconeogenesis pathway, PCK2, in mitochondria and its cytosolic isoenzyme PCK1. PCK1 was not identified by proteomics analysis, and the expression of PCK2 was not significantly changed, showing only an approximately 1.1-fold upregulation in HepG2-R cells. However, the acetylation of PCK2 at Lys-491 (K491) was increased 1.44-fold in HepG2-R cells, while acetylation of the other acetylation site of PCK2, Lys-108 (K108), was slightly increased (1.26-fold) (Fig. 3A). Notably, K108 is an acetylation site that is unique to PCK2, whereas the K491 site of PCK2 (PCK2–K491) is part of a common peptide that is shared with PCK1 and corresponds to Lys-473 (K473). Hence, because the acetylation of PCK2 at K491 was changed, we could not be rule out that the possibility that the K473 site of PCK1 (PCK1–K473) was modified.

Subsequently, Western blot analysis demonstrated that the PCK2 protein was overexpressed and that PCK1 levels were decreased in HepG2-R cells compared with their wild-type counterparts (Fig. 3B). These changes in protein expression resulted in higher total enzyme activity of PCK1/2 in sorafenib-resistant cells (Fig. 3C). The above results indicated that tolerance to sorafenib induced isoenzyme transition from PCK1 to PCK2.

3.5. PCK2 overexpression induced sorafenib resistance-related cytotoxic and metabolic phenotypes

Since PCK2, not PCK1, is the predominant PCK subtype in sorafenib-resistant cells, we observed the effects of forced expression or knockdown of PCK2 on cell sensitivity to sorafenib. As shown in Fig. 3D–F and Fig. S1, ectopic expression of PCK2 increased the IC_{50} value of sorafenib, whereas transient or stable knockdown of PCK2 decreased the IC_{50} value.

Then, HepG2-R cells were treated with the PCK1/2-specific inhibitor 3-mercaptopicolinic acid (3-MPA) alone and in combination with sorafenib. Flow cytometry analysis showed that the coadministration of 3-MPA and sorafenib exerted a synergistic effect on cell apoptosis, clonogenesis and long-term proliferation (Fig. 3G and H). Furthermore, the combination of 3-MPA and sorafenib completely inhibited mitochondrial respiration, which is an adaptive change in HepG2-R cells; in contrast, sorafenib alone slightly suppressed only spare and maximum respiratory capacity (Fig. 3I).

Additionally, we used western blotting to assess the effect of PCK2 on the expression of proteins related to the mTOR pathway in the absence or presence of sorafenib (Fig. 3J; Fig. S2). The consistent results were obtained with a previous study [24]. Collectively, these findings suggested that the isoenzyme transition from PCK1 to PCK2 was necessary for tolerance to sorafenib and metabolic reprogramming in sorafenib-resistant cells.

3.6. Reciprocal regulation of the protein stability of PCK2 and PCK1 by acetylation at PCK2–K491 or PCK1–K473 resulted in isoenzyme transition

As mentioned above, our acetylproteomics analysis revealed that acetylation of PCK2 at the K491 site was increased in HepG2-R cells (Fig. 4A). Conservation analysis indicated that K491 is a highly conserved site in mammals and is shared by the isoenzyme pair PCK1 and PCK2 in mice and humans (Fig. 4B).

To confirm this and compare the acetylation levels of PCK1/2 in HepG2-WT and HepG2-R cells, total acetylated proteins were immunoprecipitated with an anti-Ac-K antibody, and PCK1 and PCK2 were detected with specific antibodies. The results showed that the levels of the acetylated forms of PCK2 and PCK1 were significantly increased in sorafenib-resistant cells, whereas the input protein levels were increased and reduced, respectively, which is in line with the data presented in Fig. 3B (Fig. 4C). When HepG2-WT cells were exposed to a histone deacetyltransferase inhibitor (HDACi), the acetylation levels of PCK2 and PCK1 were also increased (Fig. 4D). Furthermore, the protein levels of PCK2 and PCK1 were increased and decreased, respectively (Fig. 4D

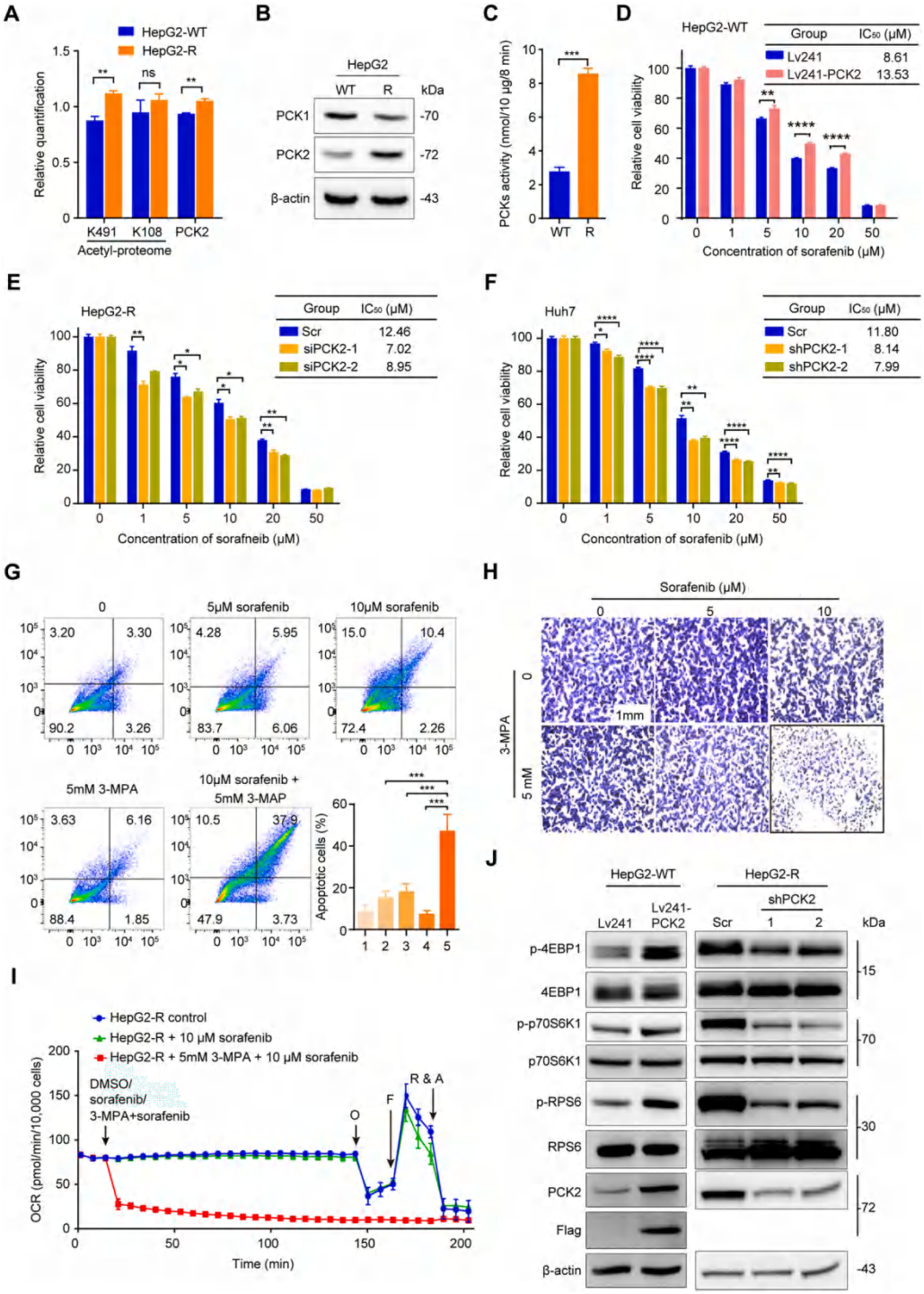

Fig. 3. Isoenzyme transition from PCK1 to PCK2 in sorafenib-resistant cells mediated sorafenib resistance in liver cancer cells. (A) The quantitative acetylproteomics and proteomics results for PCK2. Two new acetylation sites were identified in PCK2. One site, K108 is unique to PCK2, and the other site, K491, is part of a common peptide shared by PCK1 and corresponds to K473. The acetylation of this latter site was significantly increased in HepG2-R cells. (B) The expression of PCK1 and PCK2 in HepG2-WT (WT) and HepG2-R (R) cells. (C) PCK enzyme activity in HepG2-WT and HepG2-R cells. (D) Stable ectopic expression of PCK2 induced sorafenib resistance in HepG2-WT cells. The IC_{50} values of sorafenib were 8.61 μM and 13.53 μM for the empty vector Lv241 transfection group (Lv241) and PCK2 overexpression group (Lv241-PCK2), respectively. (E) Transient knockdown of PCK2 in HepG2-R cells by two specific siRNAs increased sorafenib sensitivity. The IC_{50} values were reduced from 12.46 μM in cells transfected with the scramble control (Scr) to 7.02 μM and 8.95 μM in cells transfected with siRNA-1 (siPCK-1) and siRNA-2 (siPCK2-2), respectively. (F) Stable knockdown of PCK2 in Huh7 cells transfected with two specific shRNA vectors increased sorafenib sensitivity. The IC_{50} values were reduced from 11.80 μM in cells transfected with the scramble control (Scr) to 8.14 μM and 7.99 μM in cells transfected with shRNA-1 (shPCK-1) and shRNA-2 (shPCK2-2), respectively. (G) Combination treatment with the indicated concentrations of sorafenib and the PCK inhibitor 3-MPA significantly induced apoptosis of HepG2-R cells. The apoptotic cell ratios are plotted in the bottom right panel. 1, control group; 2, 5 μM sorafenib group; 3, 10 μM sorafenib group; 4, 5 mM 3-MPA group; 5, group treated with the combination of 10 μM sorafenib and 5 mM 3-MPA. (H) Images showing crystal violet-stained HepG2-R cells treated with 0, 5 or 10 μM sorafenib alone or in combination with 0 or 5 mM 3-MPA. (I) Seahorse XF mitochondrial stress analysis of HepG2-R cells treated with control (DMSO), 10 μM sorafenib alone or a combination of 10 μM sorafenib and 5 mM 3-MPA for 3.5 h. The Y-axis represents the oxygen consumption rate (OCR, mitochondrial respiration). (J) Stable ectopic expression or knockdown of PCK2 in HepG2-WT or HepG2-R cells regulated the levels of critical proteins in the mTOR signaling pathway. Ns, not significant;

*, $P < 0.05$; **, $P < 0.01$; ***, $P < 0.001$; ****, $P < 0.0001$.

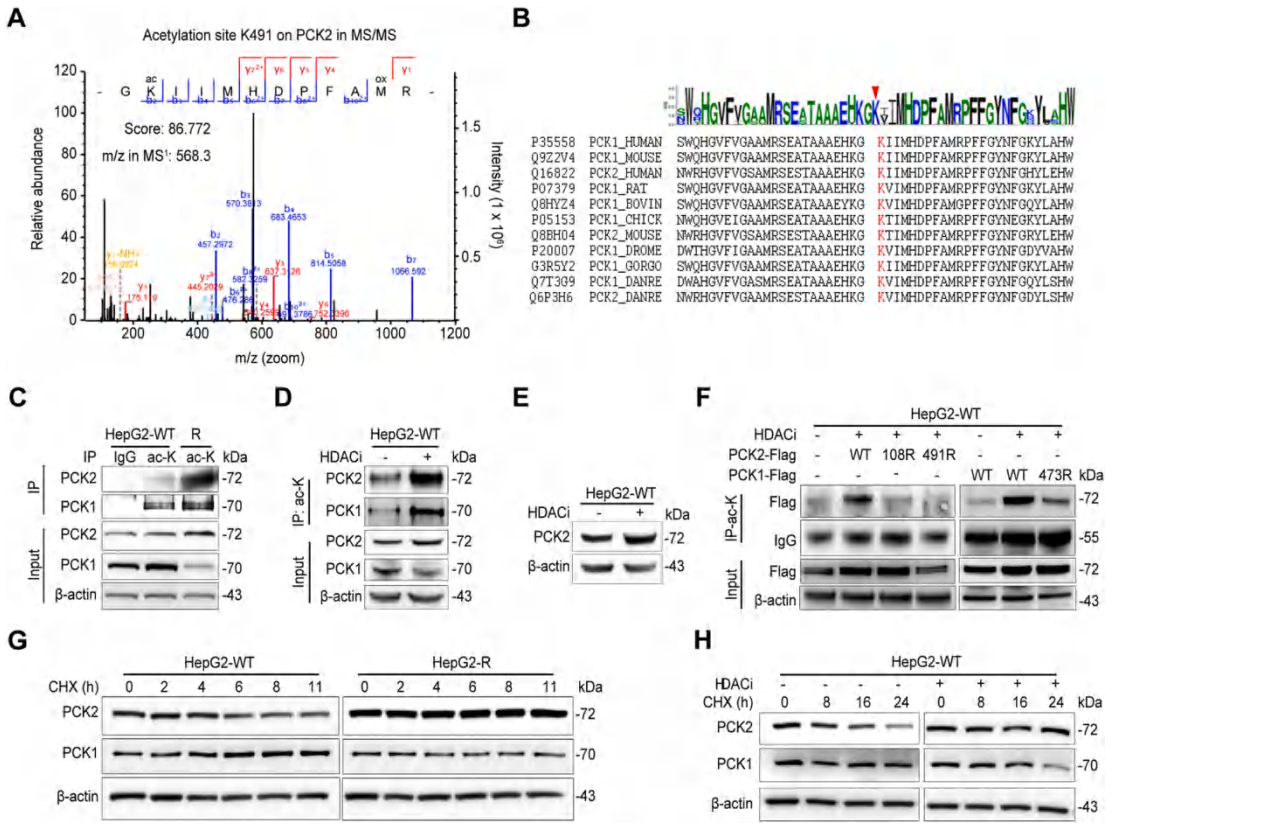

Fig. 4. Acetylation of PCK2–K491 or PCK1–K473 resulted in stabilization of PCK2 but destabilization of PCK1. (A) MS/MS spectrum of the PCK1/2 shared peptide GK(ac)IIMHDPFAMR, residues 490–101 of PCK2 and residues 472–483 of PCK, conclusively confirming that PCK2–K491 and PCK1–K473 are acetylated within this peptide. The ion type and mass/charge (*m/z*) of the observed b and y fragment ions are labeled on the peptide sequence and in the spectrum. (B) Evolutionary conservation of the PCK2–K491 acetylation site. The sequences of PCK1/2 in eight species are aligned. PCK2–K491 and PCK1–K473 are highlighted in red. (C) Endogenous acetylation levels of PCK2 and PCK1 in HepG2-WT and HepG2-R cells were measured by immunoprecipitation with an anti-pan-acetylation (ac-K) antibody followed by immunoblotting with antibodies against PCK2 and PCK1. (D) Exposure of HepG2-WT cells to HDACi enhanced the acetylation levels of PCK2 and PCK1, which were measured by IP-Western blot analysis as described. When HDACis were applied, the protein levels of PCK1 were significantly decreased, whereas PCK2 levels were slightly increased. (E) The PCK2 protein level was increased by HDACi in HepG2-WT cells. (F) Wild-type (WT) PCK2, PCK2–K108R, PCK2–K491R or PCK1–K473R was ectopically expressed in HepG2-WT cells exposed to HDACis, and the acetylation levels of PCK2 or PCK1 were measured by IP-western blot analysis. (G) Protein stability of endogenous PCK2 and PCK1 in HepG2-WT and HepG2-R cells following CHX treatment for the indicated times (in hours). PCK2 and PCK1 protein levels were measured by Western blotting. (H) HDACi stabilized endogenous PCK2 but decreased the protein stability of PCK1 in HepG2-WT cells.

and E). Additional evidence for the effect of acetylation on protein abundance was obtained in the presence or absence of HDACi in HEK 293 cells in which Flag-tagged PCK2 was ectopically expressed (Figs. S3A and B). These results suggested that increased acetylation of PCK2 and PCK1 reciprocally affected the levels of these proteins in sorafenib-resistant cells.

To further confirm that PCK2–K491, the K108 residue of PCK2 (PCK2–K108) and PCK1–K473 were acetylated in cells, we individually replaced these three sites with a nonacetylatable arginine residue (K to R mutation). Following transfection of the mutant vectors into HEK 293 cells, the overall acetylation of mutant PCK2 or PCK1 was significantly reduced compared with that of the wild-type protein (Fig. S3C), and the effect was more significant under HDACi treatment in HepG2-WT cells (Fig. 4F). Notably, expression of the PCK2–K491R mutant was significantly lower than that of the wild-type protein and PCK2–K108R protein (Fig. 4F and Fig. S3C), suggesting that K491 is a major acetylation site of PCK2 that determines protein abundance.

To address the influence of acetylation on the protein levels of PCK2 and PCK1, we first measured the protein stability of endogenous PCK2 and PCK1 under cycloheximide (CHX) treatment in HepG2-WT and HepG2-R cells in the steady state (Fig. 4G). In sorafenib-resistant cells, the stability of PCK2 was enhanced, whereas that of PCK1 was reduced, supporting the changes in protein levels described above. In the presence of HDACi, the protein stability of PCK2 was increased, whereas that of PCK1 was attenuated, indicating that acetylation stabilized PCK2 but destabilized PCK1 (Fig. 4H). Likewise, forced expression of PCK2 in HEK 293 cells had similar effects (Fig. S3D). Taken together, these results suggested that acetylation at PCK2–K491 and PCK1–K473 reciprocally regulated the protein stability of PCK2 and PCK1, leading to isoenzyme transition from PCK1 to PCK2 in sorafenib-resistant cells.

3.7. *PCK2 was acetylated at K491 by KAT8 acetyltransferase*

To identify the enzyme responsible for PCK2–K491 and PCK1–K473 acetylation, we first predicted the acetyltransferase responsible for acetylating these sites with the GPS-PAIL 2.0 tool. KAT8 was identified as a candidate. Next, we cotransfected cells with Flag-tagged PCK1 or PCK2 together with HA-tagged KAT8 or KAT5, two acetyltransferases that belong to the MYST family. Coimmunoprecipitation revealed that both PCK1 and PCK2 bound to KAT8 but not KAT5 in HEK 293 cells (Figs. S4A–C). Subsequent endogenous protein immunoprecipitation also demonstrated an interaction between PCK2 and KAT8 in HepG2-WT and HEK 293 cells (Fig. 5A and Fig. S4D). Confocal microscopy showed that PCK2 and KAT8 were definitely localized in mitochondria and that they were colocalized (Fig. 5B). Pull-down experiments further confirmed that PCK2 directly bound to KAT8 (Fig. 5C).

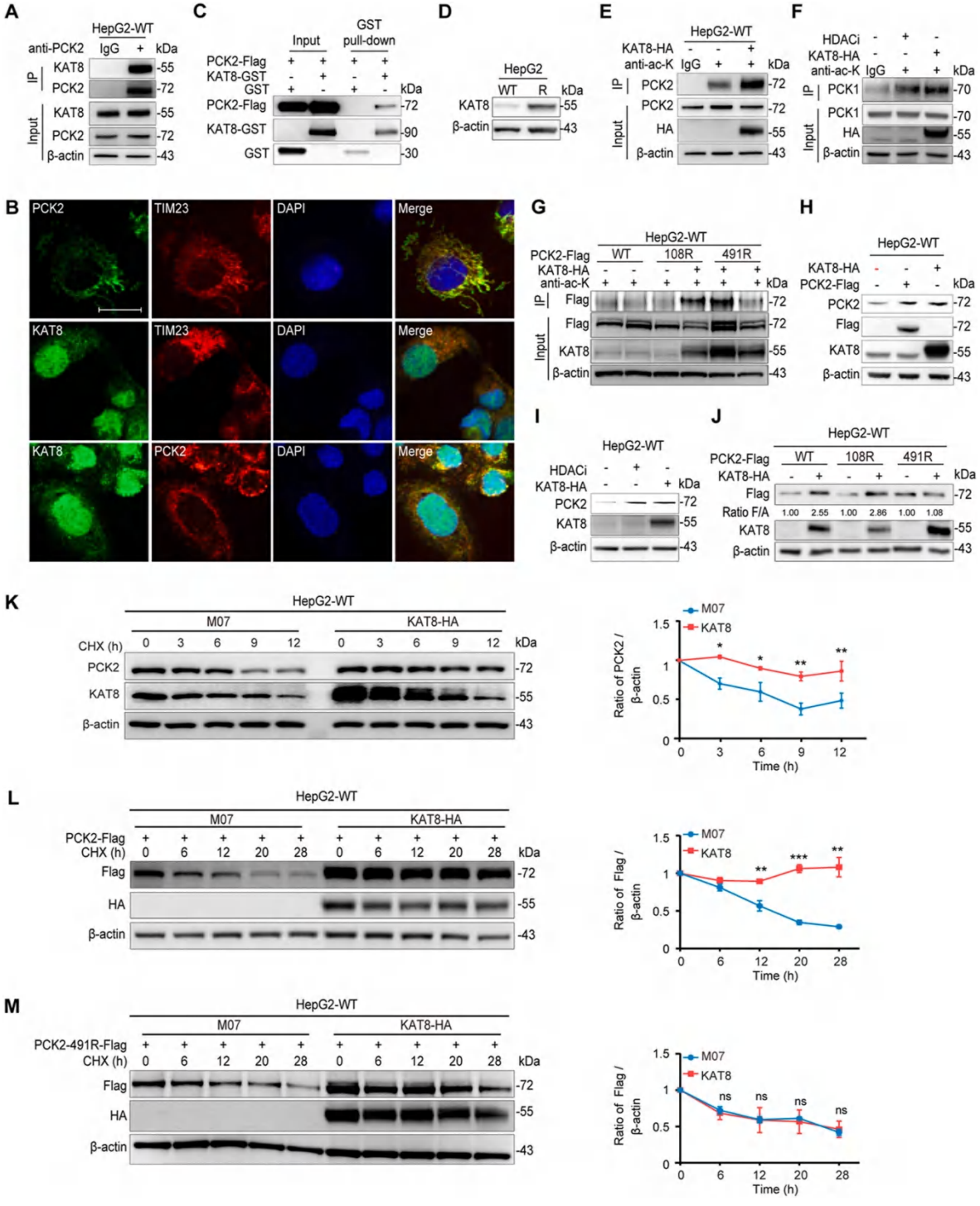

(caption on next page)

Fig. 5. KAT8-dependent acetylation of PCK2 at K491 increased protein stability. (A) Endogenous PCK2 protein bound to KAT8 in HepG2-WT cells, as determined by immunoprecipitation. (B) Analysis of the localization of PCK2 and KAT8 in mitochondria in HepG2-WT cells by confocal microscopy. Mitochondria were labeled with antibodies specific for TIM23. The nuclei were stained with DAPI (blue). (C) The interaction between KAT8 and PCK2 analyzed by a GST pull-down assay. PCK2-Flag, glutathione beads, bead-bound GST, and bead-bound GST-KAT8 proteins were mixed as indicated, and bead-bound proteins were detected by Western blotting. (D) KAT8 protein expression was upregulated in HepG2-R cells. (E) Ectopic expression of KAT8 increased the acetylation of PCK2 in HepG2-WT cells. HepG2-WT cells were transfected with a KAT8-HA-expressing plasmid, and immunoprecipitation was performed to measure the levels of acetylated PCK2 with an anti-ac-K antibody followed by Western blotting with an anti-PCK2 antibody. (F) Ectopic expression of KAT8 or exposure to HDACis increased the acetylation of PCK1 in HepG2-WT cells. (G) K491 is a major regulatory acetylation site of PCK2 that is acetylated by KAT8. Flag-tagged wild-type (WT) PCK2, PCK2–K108R and PCK2–K491R were each expressed in HepG2-WT cells, and then the cells were cotransfected with or without KAT8. Acetylation levels of PCK2 were measured by immunoprecipitation with an anti-ac-K antibody and probing with an anti-Flag antibody. (H and I) Ectopic expression of KAT8 was sufficient to increase the protein level of PCK2 in HepG2-WT cells. The effect was similar to that of forced expression of PCK2 (H) or HDACi exposure (I). (J) The effect of site-specific acetylation by KAT8 on the protein stability of PCK2. Wild-type (WT) and mutant PCK2 proteins were overexpressed in HepG2-WT cells with or without KAT8. Acetylation by KAT8 increased the stability of PCK2. PCK2–K108 did not influence acetylation by KAT8, whereas PCK2–K491 reduced the acetylation of PCK2 by KAT8, leading to attenuated protein stability. Ratio F/A, ratio of Flag and β-actin loading control. (K) Ectopically expressed KAT8 increased the stability of endogenous PCK2 in HepG2-WT cells. M07 was the empty control for the KAT8-HA vector. Each spot shows the relative band intensities of PCK2 normalized to the corresponding β-actin levels, with the ratio of the control group used for normalization. (L and M) Acetylation of PKC2 at K491 increased protein stability. Ectopically expressed KAT8 increased the protein stability of exogenous PCK2, whereas it has no effect on PCK2–K491 mutant. HepG2-WT cells were transfected with KAT8 and Flag-PCK2 or PCK2–K491R for 48 h and then treated with CHX for the indicated times. Flag-PCK2 levels were measured by western blotting. M07 was the empty control for the KAT8-HA vector. Each spot shows the relative band intensities of Flag normalized to the corresponding β-actin levels, with the ratio of the control group used for normalization.

Intriguingly, enhanced KAT8 expression, which was the molecular basis for the isoenzyme transition from PCK1 to PCK2, was also observed in HepG2-R cells (Fig. 5D). We found that ectopic expression of KAT8 enhanced the acetylation of PCK1 and PCK2 (Fig. 5E and Fig. S4E). Similar results were obtained upon HDACi treatment (Fig. 5F). Furthermore, we coexpressed KAT8 together with wild-type PCK2, PCK2–K108R or PCK2–K491R in HepG2-WT cells. We found that K491 is the major site of PCK2 that is acetylated by KAT8 because the K491R mutant dramatically diminished the acetylation levels (Fig. 5G). Collectively, these findings suggested that KAT8 is the acetyltransferase that acetylates PCK2 and PCK1 at K491 and K473, respectively, in cells.

3.8. KAT8-dependent K491 acetylation stabilized PCK2

Subsequently, we investigated whether KAT8 regulated PCK2 protein abundance and stability. The PCK2 protein level was increased by ectopically expressed KAT8 (Fig. 5H), and this effect was similar to that observed under HDACi treatment (Fig. 5I). Additionally, we found that coexpression of KAT8 and PCK2–K491R abrogated the increase in PCK2 protein expression in cells cotransfected with KAT8 and the wild-type PCK2- or PCK2–K108R-expressing vector (Fig. 5J), indicating that KAT8-dependent PCK2 acetylation at K491 impacted the protein abundance in cells. Furthermore, forced expression of KAT8 increased the stability of endogenous and exogenous PCK2 protein (Fig. 5K-M), whereas coexpression of KAT8 and PCK2–K491R had no significant effect on protein stability (Fig. 5L and M), indicating that PCK2–K491 acetylation by KAT8 was responsible for protein stability.

3.9. The nonacetylated form of PCK2 was degraded via lysosomes

To determine the degradation mechanism of the nonacetylated form of PCK2, we first treated HepG2-WT cells with the proteasome inhibitor MG-132. PCK1 protein was significantly accumulated, whereas the level of PCK2 was not increased, indicating that the deacetylation-induced degradation of PCK2 is independent of the proteasome (Fig. 6A). Thus, we exposed cells to leupeptin or chloroquine, two lysosomal protease inhibitors, and measured the level of PCK2. Marked protein accumulation was observed upon treatment (Fig. 6B). The protein stability of PCK2 was significantly increased in the presence of leupeptin (Fig. 6C). After leupeptin and/or chloroquine exposure, an increase in PCK2 levels in the lysosomal fraction was observed in HepG2-WT and Huh7 cells by Western blot analysis (Fig. 6D and E). These data suggested that PCK2 entered lysosomes for degradation.

Intriguingly, lysosomal localization of PCK2 was markedly decreased in HepG2-R cells compared with HepG2-WT cells upon leupeptin treatment (Fig. 6F). Upon simultaneous treatment with HDACi, lysosomal accumulation of PCK2 was abolished, demonstrating that acetylated PCK2 was not transported to lysosomes. Notably, ectopic expression of PCK2 in HepG2-R cells also led to lysosomal accumulation, whereas coexpression of KAT8 or exposure to HDACi inhibited this phenomenon (Fig. 6G). Moreover, because the PCK2–K491R protein could not be acetylated at K491 by KAT8, the lysosomal accumulation of the mutant protein was more obvious than that of the wild-type protein. This accumulation was not reversed by forced expression of KAT8 or HDACi treatment. The above data demonstrated that KAT8-catalyzed PCK2 acetylation at the K491 site impeded lysosomal degradation to increase the level of PCK2 in sorafenib-resistant cells.

3.10. Suppression of PCK2 restored sensitivity to sorafenib in vivo

To investigate the *in vivo* role of PCK2 in sorafenib tolerance, we established a xenograft NCG mouse model as shown in Fig. 7A. During the treatment period, mouse body weight did not change significantly in any of the groups (Fig. 7B). Intriguingly, PCK2 knockdown alone did not delay the *in vivo* growth of sorafenib-resistant cells; however, coadministration of PCK2 knockdown cells and sorafenib dramatically attenuated tumor growth (Fig. 7C and D) and markedly decreased tumor weight (Fig. 7E). The low proliferation rate of PCK2-silenced cells under sorafenib treatment was confirmed by Ki-67 staining in xenograft tumor tissues (Fig. 7F and G). These findings indicated that PCK2 itself did not inhibit tumor formation; however, depletion of PCK2 restored the response to sorafenib in mice treated with sorafenib-resistant cells.

3.11. PCK2 was a poor prognostic factor in several tumors

To evaluate whether PCK2 expression was associated with treatment outcomes in clinical samples, we first performed immunohistochemical staining of tissues from 72 patients with hepatocellular carcinoma (HCC) who received surgery followed by sorafenib treatment. As expected, PCK2 protein expression was downregulated in tumor tissues (Fig. 7H and I; Supplementary Table S4). PCK2 expression was not associated with overall survival ($P = 0.4967$; Fig. 7J). However, there was a significant correlation between high PCK2 protein levels and a shorter progression-free survival time ($P = 0.0045$; Fig. 7K). The median progression periods of the high- and low-expression groups were 2.8 and 8.1 months, respectively.

Next, we collected multiple transcriptome data from the Gene Expression Omnibus (GEO) database. Similar to what was observed for in HCC samples, PCK2 was an unfavorable prognostic factor in patients with diffuse large-B-cell lymphoma (DLBCL) receiving anthracycline-based chemotherapy regimens (the cyclophosphamide, doxorubicin, vincristine, and prednisone (CHOP)-like regimen) but not in patients treated with a CHOP-like regimen combined with rituximab immunotherapy (R–CHOP) in the GSE10846 dataset (Fig. S5A). According to the

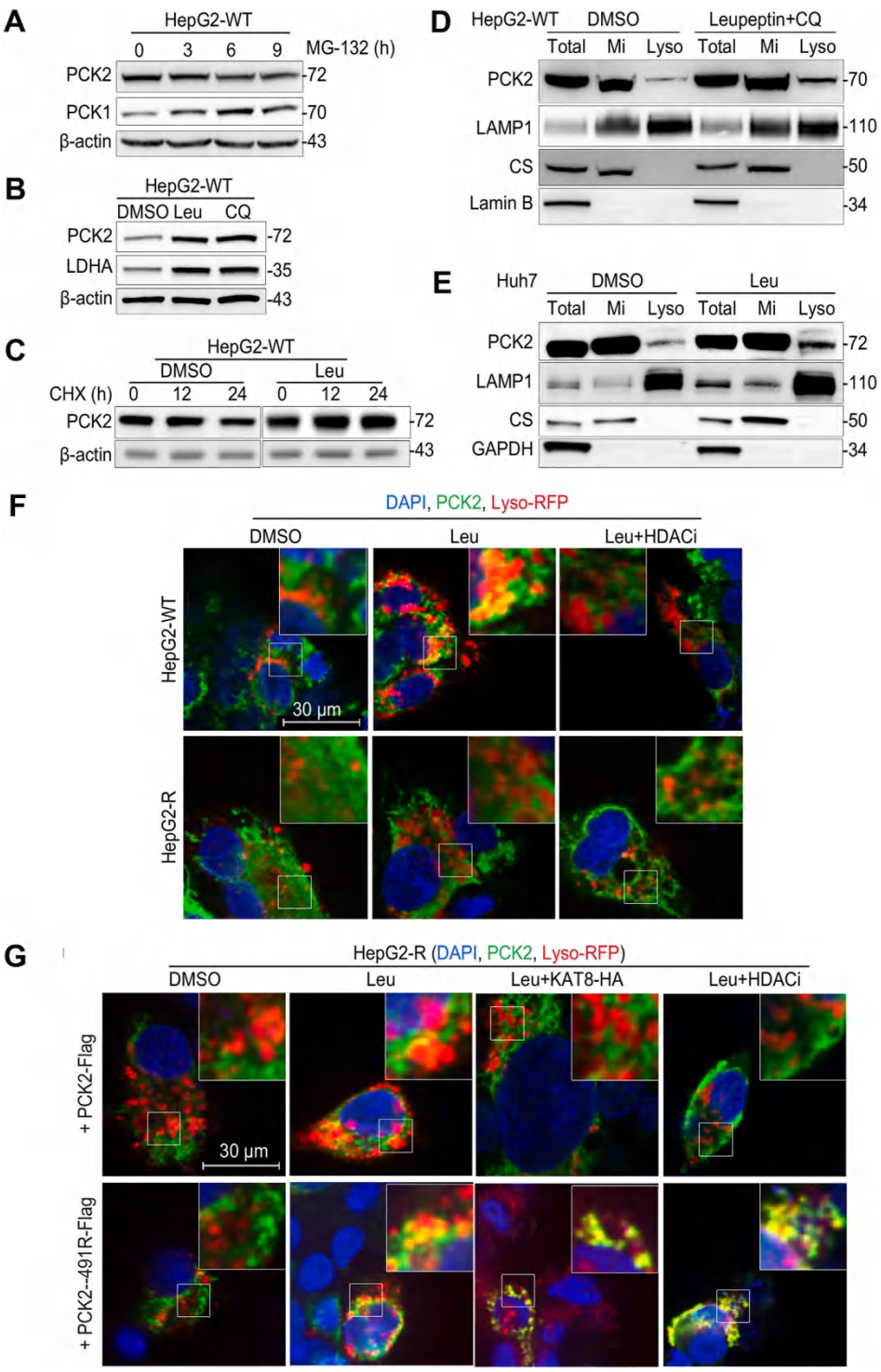

Fig. 6. Nonacetylation promoted PCK2 degradation via lysosomes. (A) PCK1 but not PCK2 was degraded by the ubiquitin-proteasome system. HepG2-WT cells were treated with the proteasome inhibitor MG132 for the indicated times, and the PCK1 and PCK2 protein levels were analyzed by Western blotting. (B) The lysosomal protease inhibitors leupeptin (Leu) and chloroquine (CQ) increased PCK2 and LDHA levels. HepG2-WT cells were treated with control (DMSO), leupeptin and chloroquine for 24 h. The PCK2 and LDHA protein levels were measured with the appropriate antibodies. LDHA, a known substrate of lysosome proteases, was used as a positive control. (C) Leupeptin stabilized the PCK2 protein. HepG2-WT cells were treated with CHX and DMSO or leupeptin at the indicated times. PCK2 protein levels were detected by Western blotting. (D–E) Subcellular localization analysis of PCK2 in HepG2-WT (D) and Huh7 (E) cells by Western blotting. Mi, mitochondrial fraction; Lyso, lysosome fraction. Lysosomal-associated membrane protein 1 (LAMP1), citrate synthase (CS) and Lamin B were used as organelle/cell compartment-specific markers for lysosomes, mitochondria and nuclei, respectively. (F) Nonacetylated PCK2 accumulated in lysosomes, as shown by confocal microscopy. Lysosomes were labeled with Lysosome-RFP reagent (Lyso-RFP, red). The nuclei were stained with DAPI (blue). Accumulated PCK2 was more abundant in lysosomes in HepG2-WT cells than in HepG2-R cells. When cells were exposed to HDACis, localization of PCK2 in lysosomes was significantly attenuated. (G) Inhibition of PCK2 acetylation at K491 promoted lysosome accumulation. Flag-tagged PCK2 or PCK2–K491R was transfected into HepG2-R cells. Confocal imaging showed that forced expression of KAT8 inhibited the localization of PCK2 in lysosomes, while the K491R mutant promoted the accumulation of PCK2 in lysosomes. Ectopically expressed KAT8 or exposure to HDACis also increased the localization of mutant PCK2 protein in lysosomes compared with that of wild-type PCK2 in lysosomes.

GSE17260 dataset (Fig. S5B), in patients with advanced-stage serous ovarian cancer (SOC) high PCK2 expression was associated with decreased overall survival time but not decreased progression-free survival time compared with low PCK2 expression. The stratified analyses demonstrated that PCK2 was a poor prognostic indicator of overall survival and progression-free survival only in patients who underwent chemotherapy after suboptimal cytoreductive surgery. In addition, in patients with lymph node-negative (GSE11121; Fig. S5C) or early-stage (GSE19783; Fig. S5D) breast cancer, PCK2 expression was a significant prognostic index for poor metastasis-free survival and disease-free survival, respectively. Taken together, these results suggested that PCK2 is an unfavorable prognostic factor for recurrence and survival in patients with various tumors, especially those receiving targeted therapy or chemotherapy.

3.12. Isoenzyme transition from PCK1 to PCK2 also occurred in lenvatinib-resistant cells

To evaluate whether the phenomenon of isoenzyme transition is unique to sorafenib resistance, we established lenvatinib-resistant HepG2 (Len-R) cells by continuously exposing cells to increasing concentrations of lenvatinib. Intriguingly, we observed decreased

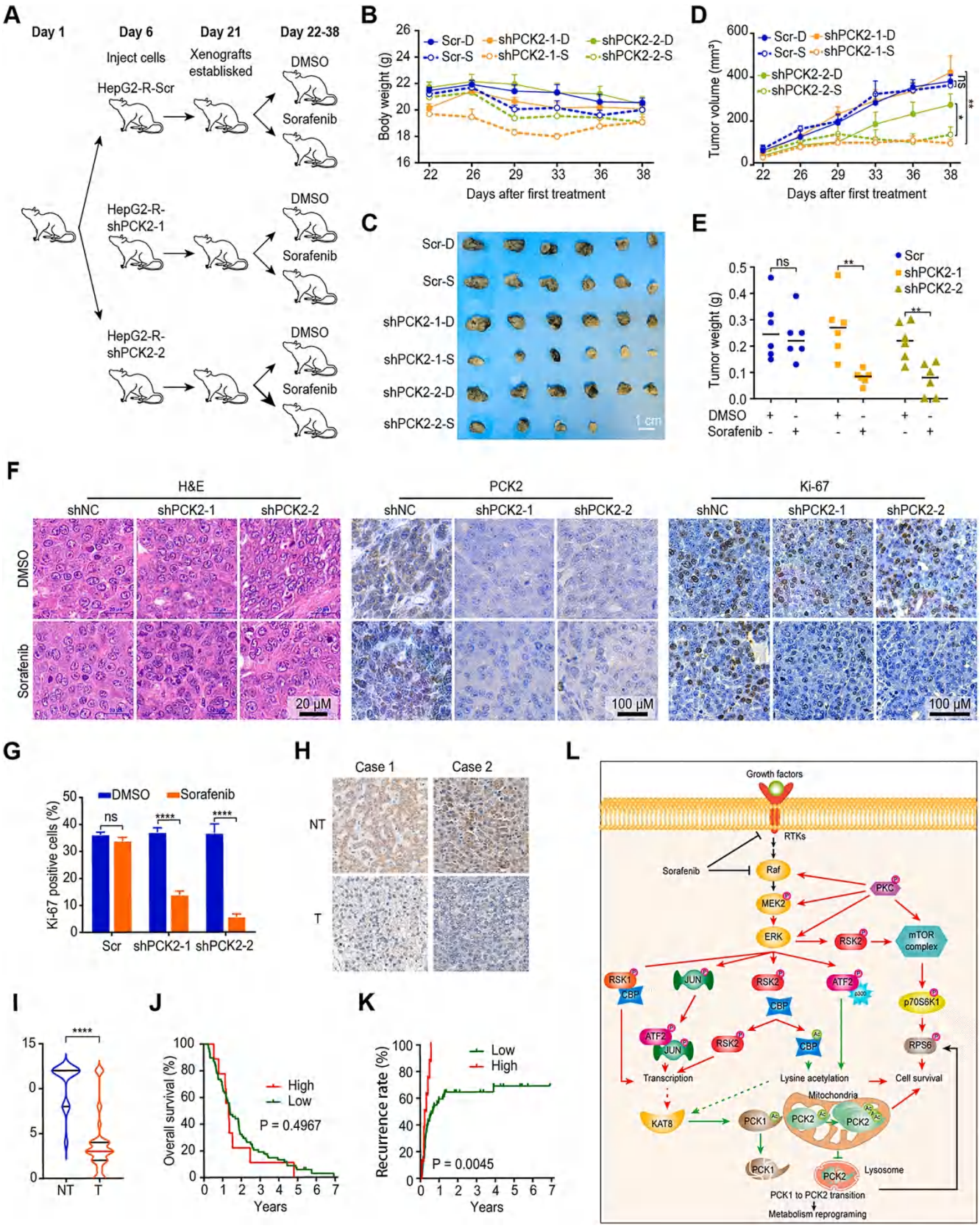

(caption on next page)

Fig. 7. Inhibition of PCK2 sensitized HepG2-R cells to sorafenib *in vivo*. (A) Schematic of the method used to establish the animal model. HepG2-R cells transfected with scramble or HepG2-R with stable PCK2 knockdown mediated by two shRNAs (shPCK2-1 and shPCK2-2) were subcutaneously transplanted into the flanks of NCG mice on day 6. After 2 weeks, tumor xenografts were established, and each group was randomly divided into two subgroups. Tumor-bearing mice were treated with control (DMSO) or sorafenib daily for 16 days. (B) Relative body weight changes in each group after treatment (n = 6). D, DMSO treatment; S, sorafenib treatment. (C) Images of tumors removed from the three groups after treatment with each agent. (D) Tumor volume (TV) was measured every two or three days, and the tumor growth curves were plotted over time until the mice were sacrificed. (E) Tumor weights in each group at the end point. (F) Images of H&E staining and immunohistochemical staining of PCK2 and Ki-67 in xenografts. (G) The percentage of Ki-67-positive cells per field in each group was calculated with ImageJ software. For (C–G), the error bars represent the standard error of the mean (SEM). ns, not significant; *, $P < 0.05$; **, $P < 0.01$; ***, $P < 0.001$. (H) Representative images of immunohistochemical staining of PCK2 in tissues from patients with HCC treated with sorafenib. NT, adjacent nontumor tissues; T, tumor tissues. Original magnification: 200 × . (I) Distribution of PCK2 protein in nontumor tissues (NT) and tumor tissues (T) determined by immunohistochemistry. The red and black lines represent the median value and 25th and 75th quartiles in each group. ****, $P < 0.0001$. (J and K) Kaplan-Meier curves of overall survival (J) and progression-free survival (K) according to the PCK2 levels in tumor samples. The log-rank test was performed. (L) A schematic diagram is shown of the regulatory network for metabolic reprogramming by sorafenib. In the schematic, the molecules in black font are proteins that were identified by our phosphoproteomics and acetylproteomics analysis and then verified by western blotting, while the molecules in gray font are proteins that were missing from the proteomics data but were subsequently validated by western blotting. Note that the alterations in protein phosphorylation caused by sorafenib affected a wide range of protein acetylation modifications in cells, leading to metabolic reprogramming. Metabolic remodeling endows sorafenib-resistant cells with a survival advantage by promoting cell proliferation and survival. The critical proteins involved in this process are PCKs. Acetylation of K491 by KAT8 acetyltransferase increases the stabilization and level of PCK2 by inhibiting its degradation in lysosomes, whereas it has an opposite effect on PCK1, leading to isoenzyme transition from cytoplasmic PCK1 to mitochondrial PCK2 in sorafenib-resistant cells. The isoenzyme transition promotes alternative carbon metabolism, including the utilization of glutamine and lactate, in mitochondria. Importantly, inhibition of PCK2 restored the sensitivity of resistant cells to sorafenib.

expression of PCK1 accompanied by increased expression of PCK2 and KAT8 (Fig. S5E), suggesting that isoenzyme transition from PCK1 to PCK2 might be a common mechanism of resistance to multiple tyrosine kinase inhibitors.

4. Discussion

Cellular metabolism must be regulated to allow a coordinated and timely response to internal and external changes. Protein post-translational modifications (PTMs) have many important attributes; they occur rapidly, are reversible, have relatively small metabolic cost, and have the ability to profoundly modulate the function of metabolic enzymes [25].

Phosphorylation is arguably the best studied PTM and is intimately involved in almost every biological process. Sorafenib is a multikinase inhibitor, and biomarkers for predicting sorafenib resistance have been identified by several studies of cell models and patient tissue and serum samples following sorafenib treatment using proteomics and phosphoproteomics analysis [26–28]. The PI3K/AKT, mTOR, HIF-1α and cell adhesion pathways might facilitate sorafenib resistance [26,28].

Acetylation is a pervasive, responsive and reversible regulator of cell metabolism that controls gene transcription and alters the activity, stability and location of metabolic enzymes [29]. Interestingly, the functions of enzyme acetylation are dependent on the modified lysine site. Acylation of different sites on the same enzyme may elicit different effects. For example, the activity of malate dehydrogenase 2 in TCA cycle can be enhanced by acylation at K185, K301, K307 and K315 but inhibited by acylation at K296 and K335 [30].

It is recognized that the suppression of mitochondrial oxidative phosphorylation is a mechanism that, similar to kinase inhibition, contributes to the antitumor activity of sorafenib [10,11]. A recent study systemically investigated the effects of short-term exposure to sorafenib on mitochondrial respiration and glycolysis in HepG2 and Huh7 cells [12]. Sorafenib significantly inhibits glycolysis, glycolytic capacity, routine respiration, electron transfer system capacity and spare respiratory capacity but increases leak respiration in a concentration-dependent manner. Moreover, it serves as an uncoupling agent to directly suppress respiratory complex I (CI) and compensatorily induce complex II (CII). Our results likewise showed that sorafenib restrained both glycolysis and mitochondrial respiration. However, sorafenib-resistant cells showed stronger glycolytic and respiratory capacity than wild-type cells, even when treated with sorafenib. The proliferation of sorafenib-resistant cells was no longer dependent on glucose, and the usage of alternative carbon sources was significantly enhanced. Thus, it seems that oxidative phosphorylation prevailed in sorafenib-resistant cells, which is consistent with previous findings [16]. The increase in the anabolic function of TCA cycle supported the notion that sorafenib induces a compensatory increase in CII activity that links oxidative phosphorylation and TCA cycle [12].

However, the mechanism of metabolic reprogramming in sorafenib-resistant cells remains unclear. Therefore, we integrated proteomics, phosphoproteomics and acetylproteomics analyses to elucidate the underlying mechanisms in this study. The results demonstrated that the differentially expressed phosphoproteins and acetylated proteins were enriched in the central carbon metabolism pathways. Importantly, the isoenzyme transition from cytosolic PCK1 to mitochondrial PCK2 mediated by acetylation was investigated in sorafenib-resistant cells.

Many metabolic enzymes in eukaryotes have isoenzymes. Despite their apparent redundancy, isoenzymes are usually evolutionarily conserved, suggesting that they make important contributions to evolutionary fitness [31]. In yeast, there are 77 metabolic isoenzyme pairs. They are enriched in central carbon metabolism pathways, and almost every reaction involved in glycolysis and gluconeogenesis can be catalyzed by two or more isoenzymes [31]. In humans, hundreds of isoenzyme pairs can form homeostatic mechanisms to facilitate allosteric regulation under a broad range of substrate profiles while requiring only a small percentage of transcriptional regulation [31,32]. Additionally, there are differences in the spatiotemporal expression of isoenzyme pairs. At different developmental stages, isoenzymes undergo phenotypic transition, with the fetal form being replaced by the adult form in adult tissues. For example, in embryonic tissues, the type BB form is the only form of phosphoglycerate mutase (PGM) and creatine kinase (CK) present, whereas during myogenesis, a complete transition from type BB to type MM occurs, leading to almost exclusive expression of type MM in adult skeletal muscle [33]. Under pathological conditions, aberrant high expression of the embryonic type or minor isoform of isoenzyme is a common phenomenon. A high level of type BB CK is required for tumorigenesis, and type BB CK acts as a prognostic indicator in numerous cancers [34]. Therefore, isoenzyme transition contributes to tumor initiation and development.

Regarding the PCK isoenzyme pair, the compartment-specific distribution of PCK1 and PCK2 in various metazoans is dependent on energy demand; PCK2 is the only isoform found in birds, whereas PCK1 accounts for 90% of PCK protein in mice and rats [21,35]. This is because PCK2 offers greater energy efficiency and requires less oxygen consumption [35]. Taken together, these findings suggest the isoenzyme transition from PCK1 to PCK2 in sorafenib-resistant cells has metabolic significance in improving energy efficiency to adapt to unfavorable environmental conditions, such as sorafenib exposure.

How do sorafenib-resistant cells achieve isoform transition from PCK1 to PCK2? Our results suggested that acetylation of PCKs catalyzed by KAT8 acetyltransferase had a reciprocal influence on their protein

stability. PCK2–K491 is located in a common peptide that is shared by PCK1. The corresponding site in PCK1 is K473. Importantly, PCK2–K481 and PCK1–K473 are located in the Ω-loop, which is essential for catalytic activity [36]. Previous studies have shown that PCK1–K473 is acetylated and confirmed that its acetylation attenuates at least 20% of its enzyme activity [37]. In addition, multiple other acetylation sites on PCK1, including K70, K71, K594, K91, K521 and K524, have also been found to affect the ubiquitin-mediated protein degradation or activity of PCK1 [37,38]. A recent study reported that lysine succinylation of PCK2 at K108 is decreased to promote migration of esophageal squamous cell carcinoma cells [39]. However, there are no relevant studies on lysine modification of PCK2 at K491 or its functions.

Our subsequent mechanistic study showed that KAT8 directly acetylated PCK2 and PCK1 at the K491 and K473 sites, respectively, and that these modifications were critical for sorafenib resistance. KAT8 is the major acetyltransferase for H4K16ac in mammals. It was previously found to partially reside in mitochondria and to have KANSL1, KANSL3 and MCRS1 as functional partners [40]. However, its effect on protein acetylation in mitochondria remains unknown. We identified PCK2 as a functional substrate for KAT8 in mitochondria. Although KAT8 was not identified by our proteomics and acetylproteomics analyses, we observed that its phosphorylation at S42 was slightly increased in HepG2-R cells (fold change = 1.104, $P = 0.0382$). It might be associated with aberrantly high expression and activity of KAT8 in sorafenib-resistant cells.

Notably, the acetylation of PCK2–K491 and PCK1–K473 had distinct effects on protein stability; that is, it diminished the lysosomal proteolysis of PCK2 but promoted the proteasomal degradation of PCK1. Acetylation of PCK1 at K70, K71 and K594 has been reported to recruit UBR5 ubiquitin ligase to ubiquitinate at K243 and K342 [38,41]. Nevertheless, due to differences in intracellular localizations, we found that the nonacetylated form of PCK2 entered lysosomes for degradation. Previous studies have shown that intact mitochondria or mitochondrial-derived compartments are eliminated via lysosome-mediated autophagy [42]. Although the mechanism of PCK2 mechanism has not been previously reported, we and others observed that PCK2 promotes the mTOR signaling pathway [24]. This suggests that it may play a role in lysosome degradation. Acetylation of PCK2 at K491 might block the recognition of sorting signals. The exact mechanism needs to be further investigated.

Furthermore, our *in vivo* experiments showed that depletion of PCK2 restored sensitivity to sorafenib, and in clinical specimens, a high level of PCK2 predicted unfavorable prognosis in patients receiving sorafenib treatment. In fact, aberrant overexpression of PCK2 has been observed in lung, stomach and breast cancers [19,43,44]. Intriguingly, compared with that in primary tumor or parent breast cancer, pancreatic cancer and prostate cancer cells, the level of PCK2 is markedly increased in metastasis- or tumor-initiating cell (TIC)-enriched tumor subclones [45–47]. Silencing of PCK2 attenuates autonomous proliferation and survival of cancer cells and mediates adaptive responses under low nutrient stress in breast cancer, lung cancer and prostate cancer [19,20,44,46]. Especially under glucose-deficient conditions, alternative carbon sources promote TCA cycle and gluconeogenesis, and the proliferation and survival of tumor cells is more dependent on PCK2 [20].

However, in gluconeogenic organs with extra high basal expression, including the liver and kidney, the expression of PCK1 and PCK2 is downregulated in tumor tissues and associated with worse survival [48,49]. In liver cancer, forced PCK1 expression promotes TCA cataplerosis, oxidative stress and apoptosis to suppress hepatocarcinogenesis under low-glucose conditions, indicating that TCA cycle is required for the survival of tumor cells [49]. Phosphorylation of PCK1 at Ser90 in liver cancer results in the phosphorylation of INSIG1/2 using GTP as a phosphate donor to restore lipogenesis and tumorigenesis; thus, phosphorylated PCK1 is associated with poor prognosis [50]. In addition, intracellular PEP can serve as a secondary messenger to regulate cytosolic calcium and NFAT activity. Overexpression of PCK1 in tumor-infiltrating T cells and PCK2 in cancer cells increases PEP production to bolster the effector functions of T cells and enhance c-myc activity by phosphorylation [51,52]. The above results demonstrate the complexity of the functions of PCK1 and PCK2. It seems that PCK2 is critical for cell survival under nutrient-deficient conditions, which are very common in tumor tissues due to hypoxia and high proliferation. Herein, it is not surprising that we found that a high level of PCK2 was associated with unfavorable prognosis in multiple cancers, especially after chemotherapy or targeted therapy.

Most importantly, the isoenzyme transition from PCK1 to PCK2 was not a coincidence in sorafenib-resistant cells. Similar results were also found in Len-R cells, indicating that the isoenzyme transition from PCK1 to PCK2 is a common mechanism that contributes to resistance to multiple tyrosine kinase inhibitors. Therefore, PCK2 could be a very promising therapeutic target for delaying acquired resistance to systemic therapy in liver cancer.

In conclusion, in the present study, we found that sorafenib induced alterations in intracellular signaling networks via phosphorylation, which in turn led to extensive acetylation changes towards a more energetic metabolic phenotype, thereby providing a survival advantage to cells with acquired resistant (Fig. 7L). Metabolic adaptation in a fluctuating nutrient environment was mediated via acetylation of PCK2–K491 and PCK1–K473 by acetyltransferase KAT8, resulting in isoenzyme transition from cytoplasmic PCK1 to mitochondrial PCK2. The inhibition of PCK2 in sorafenib-resistant cells significantly reversed drug resistance *in vitro* and *in vivo*. High levels of PCK2 predicted a shorter progression-free survival time in liver cancer patients who received sorafenib treatment. Therefore, acetylation-induced isoenzyme transition from PCK1 to PCK2 contributed to resistance to systemic therapeutic drugs in liver cancer. PCK2 is a potential novel adjuvant target for delaying the onset of acquired resistance to targeted drugs in liver cancer.

Author contributions

X.H.Z. and Y.L.S. conceived the project; Z.P.J., Y.L.S. and X.H.Z. designed the experiments; Z.P.J., J.J.G., F.F.N., J.L., L.S.T., P.N., Y.S., X. X.F., Y.Z., Y.Z., F.L. and L.P.Z. performed the experiments; Y.L.S., X.H.Z. and Z.P.J. wrote the manuscript; and all authors contributed to editing the manuscript.

Declaration of competing interest

The authors have no conflicts of interest to declare.

Acknowledgments

This work was supported in part by the National Key R & D Program (Nos. 2017ZX10203205-003-001, 2018YFC1313101 and 2016YGC0901403 to X.H.Z.), the National Natural Science Foundation (Nos. 81872033 and 82073327 to X.H.Z. and Y.L.S.) and the CAMS Innovation Fund for Medical Sciences (Nos. 2016-I2M-1-001, 2017-I2M-3–005 and 2019-I2M-1–003 to X.H.Z. and Y.L.S.) of China. We thank Ms. Xiu Dong, Lijun Yang and Meng Cai for their technical support.

Appendix B. Supplementary data

Supplementary data to this article can be found online at https://doi.org/10.1016/j.canlet.2021.06.016.

References

[1] F. Bray, J. Ferlay, I. Soerjomataram, R.L. Siegel, L.A. Torre, A. Jemal, Global cancer statistics 2018: GLOBOCAN estimates of incidence and mortality worldwide for 36 cancers in 185 countries, CA Cancer J. Clin. 68 (2018) 394–424.

[2] J.D. Yang, P. Hainaut, G.J. Gores, A. Amadou, A. Plymoth, L.R. Roberts, A global view of hepatocellular carcinoma: trends, risk, prevention and management, Nat. Rev. Gastroenterol. Hepatol. 16 (2019) 589–604.
[3] J.M. Llovet, J. Zucman-Rossi, E. Pikarsky, B. Sangro, M. Schwartz, M. Sherman, G. Gores, Hepatocellular carcinoma, Nat Rev Dis Primers 2 (2016) 16018.
[4] J.M. Llovet, S. Ricci, V. Mazzaferro, P. Hilgard, E. Gane, J.F. Blanc, A.C. de Oliveira, A. Santoro, J.L. Raoul, A. Forner, M. Schwartz, C. Porta, S. Zeuzem, L. Bolondi, T.F. Greten, P.R. Galle, J.F. Seitz, I. Borbath, D. Haussinger, T. Giannaris, M. Shan, M. Moscovici, D. Voliotis, J. Bruix, S.I.S. Group, Sorafenib in advanced hepatocellular carcinoma, N. Engl. J. Med. 359 (2008) 378–390.
[5] M. Kudo, Objective response by mRECIST is an independent prognostic factor of overall survival in systemic therapy for hepatocellular carcinoma, Liver Cancer 8 (2019) 73–77.
[6] S. Xia, Y. Pan, Y. Liang, J. Xu, X. Cai, The microenvironmental and metabolic aspects of sorafenib resistance in hepatocellular carcinoma, EBioMedicine 51 (2020) 102610.
[7] W. Tang, Z. Chen, W. Zhang, Y. Cheng, B. Zhang, F. Wu, Q. Wang, S. Wang, D. Rong, F.P. Reiter, E.N. De Toni, X. Wang, The mechanisms of sorafenib resistance in hepatocellular carcinoma: theoretical basis and therapeutic aspects, Signal Transduct Target Ther 5 (2020) 87.
[8] M. Kudo, R.S. Finn, S. Qin, K.H. Han, K. Ikeda, F. Piscaglia, A. Baron, J.W. Park, G. Han, J. Jassem, J.F. Blanc, A. Vogel, D. Komov, T.R.J. Evans, C. Lopez, C. Dutcus, M. Guo, K. Saito, S. Kraljevic, T. Tamai, M. Ren, A.L. Cheng, Lenvatinib versus sorafenib in first-line treatment of patients with unresectable hepatocellular carcinoma: a randomised phase 3 non-inferiority trial, Lancet 391 (2018) 1163–1173.
[9] D. Hanahan, R.A. Weinberg, Hallmarks of cancer: the next generation, Cell 144 (2011) 646–674.
[10] L. Fiume, M. Manerba, M. Vettraino, G. Di Stefano, Effect of sorafenib on the energy metabolism of hepatocellular carcinoma cells, Eur. J. Pharmacol. 670 (2011) 39–43.
[11] C. Zhang, Z. Liu, E. Bunker, A. Ramirez, S. Lee, Y. Peng, A.C. Tan, S.G. Eckhardt, D. A. Chapnick, X. Liu, Sorafenib targets the mitochondrial electron transport chain complexes and ATP synthase to activate the PINK1-Parkin pathway and modulate cellular drug response, J. Biol. Chem. 292 (2017) 15105–15120.
[12] J. Bai, Z. Liu, J. Liu, S. Zhang, Y. Tian, Y. Zhang, L. Ren, D. Kong, Mitochondrial metabolic study guided by proteomics analysis in hepatocellular carcinoma cells surviving long-term incubation with the highest dose of sorafenib, Aging (Albany NY) 11 (2019) 12452–12475.
[13] V. Tesori, A.C. Piscaglia, D. Samengo, M. Barba, C. Bernardini, R. Scatena, A. Pontoglio, L. Castellini, J.N. Spelbrink, G. Maulucci, M.A. Puglisi, G. Pani, A. Gasbarrini, The multikinase inhibitor Sorafenib enhances glycolysis and synergizes with glycolysis blockade for cancer cell killing, Sci. Rep. 5 (2015) 9149.
[14] H.L. Zhang, M.D. Wang, X. Zhou, C.J. Qin, G.B. Fu, L. Tang, H. Wu, S. Huang, L. H. Zhao, M. Zeng, J. Liu, D. Cao, L.N. Guo, H.Y. Wang, H.X. Yan, J. Liu, Blocking preferential glucose uptake sensitizes liver tumor-initiating cells to glucose restriction and sorafenib treatment, Canc. Lett. 388 (2017) 1–11.
[15] Y.C. Shen, D.L. Ou, C. Hsu, K.L. Lin, C.Y. Chang, C.Y. Lin, S.H. Liu, A.L. Cheng, Activating oxidative phosphorylation by a pyruvate dehydrogenase kinase inhibitor overcomes sorafenib resistance of hepatocellular carcinoma, Br. J. Canc. 108 (2013) 72–81.
[16] Y. Ren, Y.K. Gu, Z. Li, G.Z. Xu, Y.M. Zhang, M.X. Dong, Y. Wang, X.B. Zhou, CXCR3 confers sorafenib resistance of HCC cells through regulating metabolic alteration and AMPK pathway, Am J Transl Res 12 (2020) 825–836.
[17] K. Birsoy, R. Possemato, F.K. Lorbeer, E.C. Bayraktar, P. Thiru, B. Yucel, T. Wang, W.W. Chen, C.B. Clish, D.M. Sabatini, Metabolic determinants of cancer cell sensitivity to glucose limitation and biguanides, Nature 508 (2014) 108–112.
[18] G. Grasmann, E. Smolle, H. Olschewski, K. Leithner, Gluconeogenesis in cancer cells - repurposing of a starvation-induced metabolic pathway? Biochim. Biophys. Acta Rev. Canc 1872 (2019) 24–36.
[19] K. Leithner, A. Hrzenjak, M. Trotzmuller, T. Moustafa, H.C. Kofeler, C. Wohlkoenig, E. Stacher, J. Lindenmann, A.L. Harris, A. Olschewski, H. Olschewski, PCK2 activation mediates an adaptive response to glucose depletion in lung cancer, Oncogene 34 (2015) 1044–1050.
[20] E.E. Vincent, A. Sergushichev, T. Griss, M.C. Gingras, B. Samborska, T. Ntimbane, P.P. Coelho, J. Blagih, T.C. Raissi, L. Choiniere, G. Bridon, E. Loginicheva, B. R. Flynn, E.C. Thomas, J.M. Tavare, D. Avizonis, A. Pause, D.J. Elder, M. N. Artyomov, R.G. Jones, Mitochondrial phosphoenolpyruvate carboxykinase regulates metabolic adaptation and enables glucose-independent tumor growth, Mol. Cell. 60 (2015) 195–207.
[21] V. Seenappa, M.B. Joshi, K. Satyamoorthy, Intricate regulation of phosphoenolpyruvate carboxykinase (PEPCK) isoforms in normal physiology and disease, Curr. Mol. Med. 19 (2019) 247–272.
[22] J. Chen, R. Jin, J. Zhao, J. Liu, H. Ying, H. Yan, S. Zhou, Y. Liang, D. Huang, X. Liang, H. Yu, H. Lin, X. Cai, Potential molecular, cellular and microenvironmental mechanism of sorafenib resistance in hepatocellular carcinoma, Canc. Lett. 367 (2015) 1–11.
[23] Z. Wang, J. Zhou, J. Fan, S.-J. Qiu, Y. Yu, X.-W. Huang, Z.-Y. Tang, Effect of rapamycin alone and in combination with sorafenib in an orthotopic model of human hepatocellular carcinoma, Clin. Canc. Res. 14 (2008) 5124–5130.
[24] E.D. Montal, R. Dewi, K. Bhalla, L. Ou, B.J. Hwang, A.E. Ropell, C. Gordon, W. J. Liu, R.J. DeBerardinis, J. Sudderth, W. Twaddel, L.G. Boros, K.R. Shroyer, S. Duraisamy, R. Drapkin, R.S. Powers, J.M. Rohde, M.B. Boxer, K.K. Wong, G. D. Girnun, PEPCK coordinates the regulation of central carbon metabolism to promote cancer cell growth, Mol. Cell. 60 (2015) 571–583.
[25] S.J. Humphrey, D.E. James, M. Mann, Protein phosphorylation: a major switch mechanism for metabolic regulation, Trends Endocrinol. Metabol. 26 (2015) 676–687.
[26] E. Dazert, M. Colombi, T. Boldanova, S. Moes, D. Adametz, L. Quagliata, V. Roth, L. Terracciano, M.H. Heim, P. Jenoe, M.N. Hall, Quantitative proteomics and phosphoproteomics on serial tumor biopsies from a sorafenib-treated HCC patient, Proc. Natl. Acad. Sci. U. S. A. 113 (2016) 1381–1386.
[27] H. Kim, S.J. Yu, I. Yeo, Y.Y. Cho, D.H. Lee, Y. Cho, E.J. Cho, J.H. Lee, Y.J. Kim, S. Lee, J. Jun, T. Park, J.H. Yoon, Y. Kim, Prediction of response to sorafenib in hepatocellular carcinoma: a putative marker panel by multiple reaction monitoring-mass spectrometry (MRM-MS), Mol. Cell. Proteomics 16 (2017) 1312–1323.
[28] C.C. Yeh, C.H. Hsu, Y.Y. Shao, W.C. Ho, M.H. Tsai, W.C. Feng, L.P. Chow, Integrated stable isotope labeling by amino acids in cell culture (SILAC) and isobaric tags for relative and absolute quantitation (iTRAQ) quantitative proteomic analysis identifies galectin-1 as a potential biomarker for predicting sorafenib resistance in liver cancer, Mol. Cell. Proteomics 14 (2015) 1527–1545.
[29] W. Xu, Y. Li, C. Liu, S. Zhao, Protein lysine acetylation guards metabolic homeostasis to fight against cancer, Oncogene 33 (2014) 2279–2285.
[30] G.R. Wagner, D.P. Bhatt, T.M. O'Connell, J.W. Thompson, L.G. Dubois, D. S. Backos, H. Yang, G.A. Mitchell, O.R. Ilkayeva, R.D. Stevens, P.A. Grimsrud, M. D. Hirschey, A class of reactive acyl-CoA species reveals the non-enzymatic origins of protein acylation, Cell Metabol. 25 (2017) 823–837 e828.
[31] P.H. Bradley, P.A. Gibney, D. Botstein, O.G. Troyanskaya, J.D. Rabinowitz, Minor isozymes tailor yeast metabolism to carbon availability, mSystems 4 (2019) pii: e00170-00118.
[32] C. Gakis, A. Cappio-Borlino, G. Pulina, Enzymes (isoenzyme system) as homeostatic mechanisms the isoenzyme (ADA2) of adenosine deaminase of human monocytes-macrophages as a regulator of the 2'deoxyadenosine, Biochem. Mol. Biol. Int. 46 (1998) 487–494.
[33] N. Durany, J. Joseph, O.M. Jimenez, F. Climent, P.L. Fernandez, F. Rivera, J. Carreras, Phosphoglycerate mutase, 2,3-bisphosphoglycerate phosphatase, creatine kinase and enolase activity and isoenzymes in breast carcinoma, Br. J. Canc. 82 (2000) 20–27.
[34] L.M. Silverman, G.B. Dermer, M.H. Zweig, A.C. Van Steirteghem, Z.A. Tokes, Creatine kinase BB: a new tumor-associated marker, Clin. Chem. 25 (1979) 1432–1435.
[35] R. Stark, R.G. Kibbey, The mitochondrial isoform of phosphoenolpyruvate carboxykinase (PEPCK-M) and glucose homeostasis: has it been overlooked? Biochim. Biophys. Acta 1840 (2014) 1313–1330.
[36] T.A. Johnson, T. Holyoak, The Omega-loop lid domain of phosphoenolpyruvate carboxykinase is essential for catalytic function, Biochemistry 51 (2012) 9547–9559.
[37] P. Latorre-Muro, J. Baeza, E.A. Armstrong, R. Hurtado-Guerrero, F. Corzana, L. E. Wu, D.A. Sinclair, P. Lopez-Buesa, J.A. Carrodeguas, J.M. Denu, Dynamic acetylation of phosphoenolpyruvate carboxykinase toggles enzyme activity between gluconeogenic and anaplerotic reactions, Mol. Cell. 71 (2018) 718–732, e719.
[38] W. Jiang, S. Wang, M. Xiao, Y. Lin, L. Zhou, Q. Lei, Y. Xiong, K.L. Guan, S. Zhao, Acetylation regulates gluconeogenesis by promoting PEPCK1 degradation via recruiting the UBR5 ubiquitin ligase, Mol. Cell. 43 (2011) 33–44.
[39] Z. Guo, F. Pan, L. Peng, S. Tian, J. Jiao, L. Liao, C. Lu, G. Zhai, Z. Wu, H. Dong, X. Xu, J. Wu, P. Chen, X. Bai, D. Lin, L.Y. Xu, E.M. Li, K. Zhang, Systematic proteome and lysine succinylome analysis reveals the enhanced cell migration by hyposuccinylation in esophageal squamous cell cancer, Mol. Cell. Proteomics 20 (2020) 100053.
[40] A. Chatterjee, J. Seyfferth, J. Lucci, R. Gilsbach, S. Preissl, L. Bottinger, C. U. Martensson, A. Panhale, T. Stehle, O. Kretz, A.H. Sahyoun, S. Avilov, S. Eimer, L. Hein, N. Pfanner, T. Becker, A. Akhtar, MOF acetyl transferase regulates transcription and respiration in mitochondria, Cell 167 (2016) 722–738 e723.
[41] Q. Shen, Z. Qiu, W. Wu, J. Zheng, Z. Jia, Characterization of interaction and ubiquitination of phosphoenolpyruvate carboxykinase by E3 ligase UBR5, Biol Open 7 (2018), bio037366.
[42] D. Mijaljica, M. Prescott, R.J. Devenish, Different fates of mitochondria: alternative ways for degradation? Autophagy 3 (2007) 4–9.
[43] D.L. Fernandez-Coto, J. Gil, A. Hernandez, R. Herrera-Goepfert, I. Castro-Romero, E. Hernandez-Marquez, A.S. Arenas-Linares, V.T. Calderon-Sosa, M.A. Sanchez-Aleman, A. Mendez-Tenorio, S. Encarnacion-Guevara, G. Ayala, Quantitative proteomics reveals proteins involved in the progression from non-cancerous lesions to gastric cancer, J Proteomics 186 (2018) 15–27.
[44] A. Mendez-Lucas, P. Hyrossova, L. Novellasdemunt, F. Vinals, J.C. Perales, Mitochondrial phosphoenolpyruvate carboxykinase (PEPCK-M) is a pro-survival, endoplasmic reticulum (ER) stress response gene involved in tumor cell adaptation to nutrient availability, J. Biol. Chem. 289 (2014) 22090–22102.
[45] E.I. Chen, J. Hewel, J.S. Krueger, C. Tiraby, M.R. Weber, A. Kralli, K. Becker, J. R. Yates 3rd, B. Felding-Habermann, Adaptation of energy metabolism in breast cancer brain metastases, Canc. Res. 67 (2007) 1472–1486.
[46] J. Zhao, J. Li, T.W.M. Fan, S.X. Hou, Glycolytic reprogramming through PCK2 regulates tumor initiation of prostate cancer cells, Oncotarget 8 (2017) 83602–83618.
[47] N.V. Chaika, F. Yu, V. Purohit, K. Mehla, A.J. Lazenby, D. DiMaio, J.M. Anderson, J.J. Yeh, K.R. Johnson, M.A. Hollingsworth, P.K. Singh, Differential expression of metabolic genes in tumor and stromal components of primary and metastatic loci in pancreatic adenocarcinoma, PloS One 7 (2012), e32996.

[48] M.W. Khan, D. Biswas, M. Ghosh, S. Mandloi, S. Chakrabarti, P. Chakrabarti, mTORC2 controls cancer cell survival by modulating gluconeogenesis, Cell Death Dis. 1 (2015) 15016.
[49] M.X. Liu, L. Jin, S.J. Sun, P. Liu, X. Feng, Z.L. Cheng, W.R. Liu, K.L. Guan, Y.H. Shi, H.X. Yuan, Y. Xiong, Metabolic reprogramming by PCK1 promotes TCA cataplerosis, oxidative stress and apoptosis in liver cancer cells and suppresses hepatocellular carcinoma, Oncogene 37 (2018) 1637–1653.
[50] D. Xu, Z. Wang, Y. Xia, F. Shao, W. Xia, Y. Wei, X. Li, X. Qian, J.H. Lee, L. Du, Y. Zheng, G. Lv, J.S. Leu, H. Wang, D. Xing, T. Liang, M.C. Hung, Z. Lu, The gluconeogenic enzyme PCK1 phosphorylates INSIG1/2 for lipogenesis, Nature 580 (2020) 530–535.
[51] P.C. Ho, J.D. Bihuniak, A.N. Macintyre, M. Staron, X. Liu, R. Amezquita, Y.C. Tsui, G. Cui, G. Micevic, J.C. Perales, S.H. Kleinstein, E.D. Abel, K.L. Insogna, S. Feske, J. W. Locasale, M.W. Bosenberg, J.C. Rathmell, S.M. Kaech, Phosphoenolpyruvate is a metabolic checkpoint of anti-tumor T cell responses, Cell 162 (2015) 1217–1228.
[52] J. Moreno-Felici, P. Hyrossova, M. Arago, S. Rodriguez-Arevalo, P.M. Garcia-Roves, C. Escolano, J.C. Perales, Phosphoenolpyruvate from glycolysis and PEPCK regulate cancer cell fate by altering cytosolic Ca(2), Cells 9 (2019) 18.